HHS Public Access

Author manuscript

Neuroimage. Author manuscript; available in PMC 2021 April 01.

Published in final edited form as:

Neuroimage. 2011 January 01; 54(1): 60–73. doi:10.1016/j.neuroimage.2010.07.054.

BA3b and BA1 activate in a serial fashion after median nerve stimulation: Direct evidence from combining source analysis of evoked fields and cytoarchitectonic probabilistic maps

Christos Papadelis[a,b,*], **Simon B. Eickhoff**[c,d,e], **Karl Zilles**[c], **Andreas A. Ioannides**[a,f]

[a]Laboratory for Human Brain Dynamics, Brain Science Institute (BSI), RIKEN, Saitama, Japan

[b]Laboratory of Functional Neuroimaging (LNiF), Center for Mind/Brain Sciences (CIMeC), University of Trento, TN, Italy

[c]Institut für Neurowissenschaften und Medizin (INM-2), Forschungszentrum Jülich, Jülich, Germany

[d]Klinik für Psychiatrie und Psychotherapie, Universitätsklinikum RWTH Aachen, Aachen, Germany

[e]Jülich-Aachen Research Alliance (JARA-Brain), Jülich, Germany

[f]Laboratory for Human Brain Dynamics, AAI Scientific Cultural Services Ltd., Nicosia, Cyprus

Abstract

This study combines source analysis imaging data for early somatosensory processing and the probabilistic cytoarchitectonic maps (PCMs). Human somatosensory evoked fields (SEFs) were recorded by stimulating left and right median nerves. Filtering the recorded responses in different frequency ranges identified the most responsive frequency band. The short-latency averaged SEFs were analyzed using a single equivalent current dipole (ECD) model and magnetic field tomography (MFT). The identified foci of activity were superimposed with PCMs. Two major components of opposite polarity were prominent around 21 and 31 ms. A weak component around 25 ms was also identified. For the most responsive frequency band (50–150 Hz) ECD and MFT revealed one focal source at the contralateral Brodmann area 3b (BA3b) at the peak of N20. The component ~25 ms was localised in Brodmann area 1 (BA1) in 50–150 Hz. By using ECD, focal generators around 28–30 ms located initially in BA3b and 2 ms later to BA1. MFT also revealed two focal sources – one in BA3b and one in BA1 for these latencies. Our results provide direct evidence that the earliest cortical response after median nerve stimulation is generated within the contralateral BA3b. BA1 activation few milliseconds later indicates a serial mode of somatosensory processing within cytoarchitectonic SI subdivisions. Analysis of non-invasive magnetoencephalography (MEG) data and the use of PCMs allow unambiguous and quantitative (probabilistic) interpretation of cytoarchitectonic identity of activated areas following median nerve stimulation, even with the simple ECD model, but only when the model fits the data extremely well.

[*]Corresponding author. Center for Mind/Brain Sciences (CIMeC), Laboratory of Functional Neuroimaging (LNiF), Via delle Regole 101, 38100 Mattarello (TN), Italy. Fax: +39 0461 882521. christos.papadelis@unitn.it (C. Papadelis).

Keywords

Somatosensory evoked fields; Serial processing; Median nerve; Cytoarchitectonic probabilistic maps

Introduction

The somatosensory evoked responses have long been used in the study of physiology and pathophysiology of the human somatosensory system. They represent measurements of brain activity elicited by stimulation of peripheral nerves, and can be recorded noninvasively using either electroencephalography (EEG) or magnetoencephalography (MEG) that provide a millisecond temporal resolution. Bipolar transcutaneous electrical stimuli, that are technically less demanding than vibratory or tactile stimuli, are usually applied on the skin over the trajectory of the median nerve producing strong and well-defined MEG and EEG waveforms. The putative superiority of MEG to EEG is largely based on MEG being practically unaffected by the detailed structure and conductivity of the skull and scalp.

The recorded SEFs following median nerve stimulation are generally classified by their post-stimulus latencies, as short-latency responses (less than 40 ms after stimulus onset), and long-latency responses (40–300 ms after stimulus onset). The morphology of the short-latency SEFs has been consistently reported as two prominent peaks of opposite polarity, one around 20±1 ms (N20) and the second at 32±3 ms (P30) (Hari et al., 1984; Kawamura et al., 1996; Mauguière et al., 1997 Mima et al., 1998; Rossini et al., 1996; Tecchio et al., 1997). Secondary, masked, short-latency responses have been observed at 25 ms (P25) and 35 ms after subtracting the neural activity that is responsible for the two prominent components N20 and P30 from the recorded waveforms (Inui et al., 2004).

In addition to the millisecond temporal resolution that allows us to explore the timing of basic neural processes at the level of cell assemblies, MEG offers a very good localisation accuracy of a few millimeters especially for superficial cortical sources such as those located in the primary somatosensory cortex. It has thus been successfully used for the localisation of neural sources activated during somatosensory processing after median nerve stimulation (Inui et al., 2004; Kakigi, 1994; Kawamura et al., 1996; Tecchio et al., 2000; Tiihonen et al., 1989). The good localisation accuracy of MEG has been confirmed by realistically head-shaped phantom studies (Leahy et al., 1998; Papadelis et al., 2009). In these studies, superficial sources were localised with an accuracy of 2–3 mm by using different inverse methods.

The anatomic generators of short-latency human somatosensory responses have been the subject of considerable debate. Although there is a general agreement that some portion of the spatio-temporal SEFs originates in the somatosensory cortex on the postcentral gyrus, there is disagreement about the specific regions involved. The earliest cortical response component after median nerve stimulation (N20) is considered to be generated in area 3b contralateral to the stimulated arm based on its macroanatomical location (Allison et al., 1989; Baumgartner et al., 1991; Buchner et al., 1994; Hari et al., 1984; Wood et al., 1985). Cortical surface and laminar recordings in macaca monkeys support further this notion

(McCarthy et al., 1991). The origin of the following restricted reflection P25 is debated. It is generally considered to be located in BA1 (Inui et al., 2004; Kakigi, 1994), though other studies considered it of precentral (motor cortical) origin because the sources are typically more anterior compared to N20 (Kawamura et al., 1996; Tiihonen et al., 1989). Huttunen (1997), however, argued that this finding resulted from a modeling error rather than from an additional generator in the precentral motor cortex. The P30 component seems to be generated in the contralateral SI (Wikström et al., 1996), most probably reflecting early inhibitory postsynaptic potentials, while more recent reports locate it in BA3b (Inui et al., 2004). It is important to stress that the results from these earlier human studies were reached on the basis of gross landmarks and expectations derived from invasive recordings in animals (McCarthy et al., 1991).

Spatial normalization of individual anatomical images and follow up reference to a common anatomical space such as the MNI reference system (Evans et al., 1992) is practiced widely despite its approximate nature because of considerable intersubject variability and absence of a genuine microstructural foundation on the examined subjects (Eickhoff et al., 2005). Alternatively, the use of macroanatomical landmarks provides in some cases a reliable framework for establishing structure-function relationships (Amiez and Petrides, 2009; Dumoulin et al., 2000; Tootell et al., 1995; Zeki et al., 1991). Reference to macroanatomical landmarks, however, is not quantitative and for the borders of most cortical areas there are simply no such landmarks, because the sulcal and gyral pattern is highly variable across subjects (Amunts et al., 1999, 2000; Amunts and Zilles, 2001). Only in the visual system precise retinotopic mapping provides a reliable and quantitative guide of cytoarchitectonic identity of areas (cf. Wilms et al., 2005, 2010), as already exploited in many fMRI studies and our earlier study of MEG/fMRI localisation accuracy (Moradi et al., 2003).

A quantitative cytoarchitectonic reference for regionally specific activations observed in functional imaging studies is provided by microstructurally defined areas (Bodegård et al., 2000, 2003; Amunts et al., 2004; Eickhoff et al., 2005, 2007, 2008; Wohlschläger et al., 2005; Zilles and Amunts 2010). PCMs provide this microstructural stereotactic information on MNI reference space while allowing for the variability of cortical areas across subjects (Amunts and Zilles, 2001; Mohlberg et al., 2003; Zilles et al., 2002). This approach provides characterization at specific location while overcoming many of the problems of classical cytoarchitectonic maps (e.g., Brodmann, 1909; Zilles and Amunts, 2010). Such maps have been published for various brain regions, including the primary (Geyer et al., 1999, 2000; Grefkes et al., 2001) and secondary (Eickhoff et al., 2006a,b) somatosensory cortex. The PCMs are based on the observer independent analysis of the cytoarchitecture in a sample of ten human post-mortem brains (Schleicher et al., 2005). In the last few years, PCMs have been successfully applied in functional imaging studies using positron emission tomography (PET) (Geyer et al., 1996, 2001; Horwitz et al., 2003; Young et al., 2003), functional magnetic resonance imaging (fMRI) (Amunts et al., 2004; Binkofski et al., 2000; Bodegård et al., 2000, 2003; Eickhoff et al., 2006b, 2008; Heim et al., 2005; Jakobs et al., 2009; Wohlschläger et al., 2005), and MEG (Barnikol et al., 2006; Dammers et al., 2007; Prieto et al., 2007). These applications not only demonstrated the feasibility of the probabilistic integration of anatomical and functional data but moreover demonstrated the additional level of structure–function inference permitted by it.

The main goal of this study is to relate focal generators identified in the localisation analysis of short-latency SEFs to the cytoarchitectonic organization of the somatosensory cortex as described by the PCMs. The study is confined to the analysis of averaged MEG data, filtered in different frequency bands. SEFs elicited by median nerve stimulation were recorded in humans. The single ECD was used for modeling the averaged data, since it is widely used and produces good fits to the average data when a single focal generator is primarily responsible for the generation of the MEG signal (Papadelis et al., 2009). The identified foci of activity were transformed onto the MNI space and then were superimposed with cytoarchitectonic probability maps. It was hypothesized that the cortically evoked responses will involve excitation of well-defined cytoarchitectonic areas and would thus lead to focal activations. We assumed that in general the activity in different cytoarchitectonic areas may overlap in time, but in some time-points the activity from one of these areas would dominate. At these time-points, the goodness of fit (GOF) of instantaneous ECD estimates of cortical activities would be high, and the probabilistic assignment of the cytoarchitectonic area would have high probability to be in one of the main cytoarchitectonic areas. In order to verify the source localisation results based on dipole source analysis, MFT (Ioannides et al., 1990), a tomographic imaging approach, was also applied. The MFT algorithm uses optimally information from the MEG sensors around the head relying minimally on a priori assumptions about the nature of the generators. From the theoretical point of view, it was shown to localise distributed sources and allow for sharp changes in the distribution density so that focal generators can be accommodated (Taylor et al., 1999); at the practical level it was also demonstrated in numerous applications that MFT can deal effectively with both diffuse and focal current densities in the brain (Ioannides 1995, 2006). It therefore follows that at latencies corresponding to poor ECD solutions, MFT solutions will be either more spread or the activity will be present simultaneously in different cytoarchitectonic areas. In contrast at the time-points when ECD gives a good fit to the data and MFT identifies a focal solution (coinciding with the ECD location) the identified generator is likely to correspond to activation of a single cytoarchitectonic area. Some of the early MFT studies, using MEG data from only part of the head have suggested that the ECD solutions are likely to be reliable if the MEG data are fitted with a goodness of fit of 0.97 or higher (Ioannides et al., 1990, 1993a,b). The question to be addressed in this paper is how this translates to the better quality data from modern full-head MEG systems and whether or not an accurate ECD estimate when a single focal generator is present is reflected in a higher probability for one cytoarchitectonic area in the PCM.

Material and methods

Subjects and measurements

Six healthy right-handed subjects (five males and one female; age: 30.83±6.58 years) participated in a somatosensory experiment. Ethical committee approval was obtained from the RIKEN Ethics Committee and subjects gave written informed consent before the experiment. The median nerve was electrically stimulated transcutaneously on the right and left wrists. Two electrodes (cathode proximal) were connected directly to the photoelectric stimulus isolation unit of our electrical stimulator (Grass Model S8800). Before the experiment, the motor threshold (MTH, the minimal stimulus intensity required to produce

thumb movement), and the sensory threshold (STH, the minimal stimulus intensity corresponding to the level at which the subject was just able to feel a train of stimulus pulses, repeated four times) were determined for each wrist. MTH and STH stimuli were 6.8±2.1 mA (mean±S.D.) and 2.3±1.9 mA respectively. During the experiment, the subject was comfortably seated under the MEG helmet keeping his/her head still. The arms were well covered to prevent cooling throughout the recording session. Constant current stimuli with a duration of 0.2 ms, and pseudo-randomized inter-stimulus interval of 600±100 ms were used. Four data runs were collected for each subject, with 120 stimuli delivered in each run. The stimuli were delivered to the right wrist in two runs and to the left in the other two. The stimulus intensity was $M = MTH + 0.25 \cdot \Delta$, where $\Delta = MTH - STH$ (Ioannides et al., 2002), sufficient to provoke a painless thumb twitch. A ground band was placed round the forearm above the stimulating electrodes in order to minimize the artifactual magnetic fields caused by the stimulus current. The subjects kept their eyes open and fixated on a small cross during the experiment.

SEFs were recorded using the CTF (VSM MedTech Ltd) whole head system (151 channels) at a sampling rate of 1250 Hz, together with the vertical and horizontal electrooculogram (EOG), and electrocardiogram (ECG). The CTF system uses radial gradiometers as primary sensors. Hardware filters were adjusted to band-pass the MEG signal, 0–400 Hz. Standard CTF software was used offline to process the data digitally by using a 3rd order gradient filter, a 50 Hz notch filter (and its harmonics), and by removing the DC.

SEFs data preprocessing and virtual channels

The recorded MEG signal was visually inspected for possible artifacts. The INFOMAX algorithm (Lee et al., 1999) for independent component analysis (ICA) in conjunction with the EOG and ECG data was used to remove eye blink and cardiac artifacts. The recorded responses were initially filtered offline (butterworth, 4th order) in the frequency band of 0–250 Hz (whole-band). The filtered 120 trials were then averaged for each separate run from −20 to 100 ms relative to the stimulus onset.

A virtual channel was defined for each run from the contour map of each subject's averaged data showing the iso-magnetic field during the N20 peak (see Fig. 1, upper left panel). The virtual channel was estimated by the difference between the MEG signals from sensors covering the peak magnetic flux entering the head and exiting the head. In general the reduced dimension of virtual channel is less sensitive to noise that is uncorrelated among channels (Gross and Ioannides, 1999). This is due to the linear transformation, which is essentially a weighted averaging of the original channel signals, so that uncorrelated noise is reduced. For details of the definition of virtual channel and its applications see Liu et al (1998).

Signal-noise-ratio (SNR)

Two standard measures of reproducibility across trials, the signal-noise-ratio (SNR) and the intertrial synchronization index (ITS) (Laskaris et al., 2003), were calculated for the virtual channel of each run. Each of these measures was computed for a moving window thus

providing a time-dependent quantification of the signal content of the ensemble of single trials (STs). The SNR for this window is defined as follows (Laskaris and Ioannides, 2001):

$$SNR = \frac{SP}{NP},$$

where the $SP = \frac{1}{p}\|\bar{x}\|_{L_2}^2 - \frac{1}{N}NP$ is the signal power (SP) and the $NP = \frac{\sum_{i=1}^{N} \|\bar{x} - x_i(t,p)\|_{L_2}^2}{p(N-1)}$ is the noise power (NP) of the averaged signal $\bar{x} = \frac{\sum_{i=1}^{N} x_i(t,p)}{N}$ .The $\bar{x}$ is the ensemble average of N ST patterns, each with p samples and time between samples t. The NP is the ensemble average of ST deviations from $\bar{x}$, computed with the L_2 norm. The SP is the noise-corrected L_2 norm of $\bar{x}$. The SNR can be thought of as the ratio of the "energy" in the reproducible part of the signal divided by the "energy" of the residual signal across STs.

Time-frequency analysis

Time-frequency representation maps were estimated for the SEFs of each subject by computing the spectrogram distribution of the virtual channel (averaged data between the two runs of each side). The spectrogram distribution corresponds to the squared modulus of the short-time Fourier transform:

$$S_x(t,\upsilon) = \left| \int_{-\infty}^{+\infty} \bar{x}(u) \cdot h^*(u-t) e^{-j2\pi\upsilon u} du \right|^2$$

where h is the smoothing window function (here Hamming window), and x is the ensemble average of N ST patterns of the virtual channel. The analysis was performed in Matlab by using the Time-Frequency Toolbox (http://tftb.nongnu.org/). In most runs, the energy spectral density of the virtual channel signal for the early latency responses (during the first 100 ms after stimulus onset) separated into two components. The first component was brief lasting only about 10–15 ms centered around 20 ms; this component showed the expected suppression of low rhythms (below 15 Hz) and had high energy content in the frequency range from 50 to 150 Hz. The second component was stronger around 30–40 ms (extending from about 25 to 90 ms) and it was dominated by low frequencies with little energy for frequencies above 50 Hz (see Fig. 1).

Filtering

In order to increase the SNR of the MEG signal and hereby to improve the accuracy of subsequent dipole localisation, we digitally filtered (butterworth, 4th order) the recorded responses offline in three different frequency bands: (a) 0–50 Hz (low-band), (b) 50–150 Hz (medium-band), and (c) 150–250 Hz (high-band). The selection of the frequency bands was based on the results of our time-frequency analysis and the unavoidable effect of the 50 Hz notch filter (and its harmonics). Since our main interest was the short-latency responses to the median nerve stimulation, we tried to improve the SNR within this time window by filtering the data. The high-band was included in the analysis in order to capture possible

high-frequency oscillations that have been previously observed to superimpose on the N20 component in this frequency band (Haueisen et al., 2001; Papadelis et al., 2009). The filtered data of each separate frequency band were then averaged for each run from −20 to 100 ms relative to the stimulus onset.

Peak amplitudes and latencies were measured on the averaged MEG signals for each run and each frequency band including the whole-band. The components that showed a latency with standard deviation <4 ms and identified in at least three subjects were retained for further analysis.

The time-frequency analysis results suggest that for transitions within and close to SI for the early responses the frequency range from 50 to 150 Hz provides the best view on early interchanges of activity between areas. By filtering the MEG data in this frequency band, we reduced both ambient field noise and brain activity that is uncorrelated with the stimulus. We thus increased the SNR of the recorded MEG signal using the applied filters (see details later in the Results section). High values of SNR then allow better localisation of the underlying neural sources (Moradi et al., 2003; Poghosyan and Ioannides 2008).

Source analysis

The single ECD model was used to analyze the averaged data. This method allows the spatio-temporal modeling of neural sources over defined intervals assuming that one focal source generates the observed magnetic activity. The source is described by an infinitesimally small line element (Hämäläinen et al., 1993). The location, orientation, and moment of the dipole were calculated by an iterative least-square fit. The GOF indicates the percentage of the data that can be explained by the model, and was estimated as GOF (%) = 100–Error. The Error value (%) was defined as follows:

$$Error(\%) = 100 \times \frac{\sum_{i=1}^{N} \frac{\left(B_i - B_j'\right)^2}{Var_i}}{(N - D)}$$

where N was the number of sensors, B the observed signal at sensor i, B' the calculated signal at sensor i, Var_i the variance, and D the number of free parameters. We considered ECD models with error values lower than 10%. The ECD modeling was performed at each timeslice (in steps of 0.8 ms) from 10 to 40 ms. To describe the head conductivity, the multiple local spheres model was used. It uses a different local sphere for each MEG sensor to fit the curvature of the inner skull surface just below the sensor. For the ECD analysis, the latest version (Version 5.4.0 – linux-20061212) of the CTF (VSM MedTech Ltd, BC, Canada) software was used.

We used MFT (Ioannides et al., 1990; Taylor et al., 1999) to obtain a more general description of the generators than what the ECD model provides. MFT relies on a non-linear algorithm with optimal properties for tomographic analysis of the MEG signal so that the details in the data determine whether a solution is focal or not. MFT computes the 3D distribution of primary current density vectors throughout the brain at each timeslice (in our case every 0.8 ms). In the present study, MFT solutions were calculated for the averaged

MEG data of each run at each timeslice from 10 to 40 ms. For the MFT analysis, an in-house software was used.

Monte-Carlo simulations

In order to quantify the confidence regions of our ECD localisation results, we estimated the confidence volume (ellipsoid) of the ECD fits at the peak of N20 component for each run and each subject. The confidence volume was based on Monte-Carlo simulations and its calculation was performed by the standard CTF software. Monte-Carlo simulations were performed only on the whole-band averaged data. As nominal dipole configuration was used the single dipole fit at the peak of N20. Gaussian distributed noise with given variance was added to the MEG of each sensor *i*:

$$noise_i = k \cdot \sqrt{Var_i}$$

where Var_i is the variance of the MEG signal at sensor *i*, and *k* is a random number from −0.5 to 0.5. Then a dipole fit was performed on the noisy data. Because of the added noise, the resulting dipole solution is slightly shifted relative to the localisation without the added noise. This procedure was repeated 500 times, producing a ‘dipole cloud’ for each case. For each dipole cloud, we computed the center of gravity of all points in the cloud, and determined an ellipsoid, with origin the center of gravity, that encompass 95% of the estimated dipole points.

Simulation data

The ECD is expected to work well for superficial focal sources as those that might be activated at early latencies during somatosensory processing; at these latencies high values of GOF are expected. Conversely, high GOF values indicate that the MEG signal is dominated by the contribution from a single focal source; at these time-points, other possibly simultaneously active sources are either uncorrelated with the stimulus and thus reduced by averaging or they are long-lasting and therefore more likely to overlap with components that have been removed by filtering.

In order to validate the reliability of our methodological approach, simulation data were generated using two simultaneously active dipolar sources. The Dipole Simulator (Version 3.2) was used for the generation of these data. Two cases were examined where the two sources namely S_1 and S_2 were either perfectly synchronized or having a few millisecond difference in their respective activation patterns (see Fig. 2). They were placed within the left motor and primary somatosensory areas respectively, separated from each other by 5 mm. Simulated noise was added to the data (RMS noise = 15 fT) in order to render them similar to the background MEG signal. The moment and orientation of each source was adjusted to produce a magnetic field at the sensor level within the physiological range. Fifty trials of magnetic fields were generated for each case. The simulated data were preprocessed as the human SEFs, filtered in the 0–250 Hz frequency band, and averaged. The single ECD model was used to analyze the averaged data as was the case in the main study.

Co-registration of MEG and MRI

The subjects' heads were scanned with a high-resolution anatomical MRI (1.5 T MRI, Model ExcelArt, Toshiba Medical Systems) using a T1-weighted volume acquisition sequence resulting in a voxel-size of 1×1×1 mm^3. The coordinates of MEG sensors were determined relative to the individual subject MRI for each run by the localisation of fiduciary coils and an in-house co-registration procedure (Hironaga and Ioannides, 2002). Before the MEG experiment, three head coils were attached to the subject's scalp (nasion, left and right preauricular points). The three coils defined a coil-based coordinate system. Two extra coils were also attached to the right and left forehead. The surface of the head and face, with all five coils, was digitalized using a 3D non-contact laser scanner (VIVID 700, Konica Minolta, Japan) and the scalp with a 3D digitizer (Polhemus, 3Space/Fastrak, USA). The digitized head shape information was fitted to the subject's MRI to obtain a transformation matrix between the coil- and MRI-based coordinate systems. The relative positions of the five coils were found by measuring the generated magnetic field. The two extra coils were then removed. The three fiduciary coils were activated at the beginning and end of each experimental run and so the precise position of the brain relative to the sensors for each run was known. The results for the co-registration were checked manually, and if the fit was not accurate the digitization process was repeated. Co-registration was regarded as accurate, if the mean distance between the surface of the head and face derived from the 3D laser scanner, the 3D digitizer, and the anatomical scan was <2 mm.

PCMs

Analysis solutions were always referred to the source space defined by the subject's brain. To identify the cytoarchitectonic area of the underlying neural activity, the localisation estimates of the SEFs for both ECD and MFT were compared to the PCMs solutions for each time-point of each run. To transform the functional solutions defined on the source space of each subject's brain, the T1 images of the individual subjects were spatially normalized to the MNI single subject template using the "unified segmentation" approach (Ashburner and Friston, 2005). The resulting parameters of a discrete cosine transform, which define the deformation field necessary to move the subject's data into the space of the MNI tissue probability maps, were then combined with the deformation field transforming between the latter and the MNI single subject template where the PCMs are located. The ensuing deformation was subsequently applied to the localisation estimates that were hereby transformed into the space of the PCMs. The public domain software 'Anatomy Toolbox' software (v1.5) (Eickhoff et al., 2005, 2006a, 2007) was used for assessing the histological correlates of the functional imaging results.

Results

Source localisation of simulation data

We will describe in this subsection the behavior of the estimated dipole in time for the two cases of the simulation data. When the two simulated sources S_1 and S_2 were activated with only partial temporal overlap, the ECD initially approached the actual location of the first source (Fig. 2, upper panel). At these time-points the GOF was very high, reaching values >98%. Few milliseconds later when the second source was activated, the dipole moved

between the two sources, away from S1 gradually approaching the location of S2. When the two sources were almost equally strong (~33 ms), the error was almost double, though still only about 4%, and the estimated dipole was located somewhere between the two actual sources (Fig. 2, upper panel). The same level of error was observed when the two sources were perfectly synchronous (Fig. 2, lower panel).

The SEFs morphology

Here only responses observed contralaterally to the stimulus side are considered. We will describe in this subsection the main features of the averaged evoked responses, as these can be determined from the analysis in different frequency ranges of the raw MEG signal and linear combinations of the signal from different channels. To avoid crowding the text with too many numbers we will list the latency details of the different components separately in Table 1.

The whole-band (0–250 Hz) average SEFs were characterized by a complex morphology. Two major short-latency components of opposite polarity were prominent in all subjects around 21 (C1) and 31 ms (C3) (Fig. 3 — first panel). A weak component around 25 ms (C2) was also identified in four out of six subjects (Table 1). In all subjects, a fourth component was observed (C4); in four of them it was between 40 and 50 ms (Fig. 3 — first panel), in the remaining subjects much later around 70 ms. The short-latency components were followed by a broad slow component peaking between 51.2 and 93.6 ms, which could be identified in all examined subjects (Fig. 3 — first panel). The peak latency of this late component showed high inter-individual variations. The field maps showed a dipolar pattern over the contralateral somatosensory cortex at around 21 ms (Fig. 1 — left upper panel) that presented an opposite polarity around 30 ms. At the time-point of weak component around 25 ms, the field map showed a similar dipolar pattern as at 20 ms but rotated clockwise ~30°.

In the low-band, there was only one clearly defined component at short-latencies (<40 ms) around 34 ms (CL1) (see Table 1 for latency details) for the MEG signal (butterfly plot) (Fig. 3 — second panel). Slow components were observed in all subjects at later latencies for this frequency band. The filtered SEFs in the medium-band were characterized by a more complex but clearer morphology than the whole-band data. Four major components (CM1–4) were identified in the short-latencies around 16, 21, 25 and 30 ms (see Table 1 for latency details) (Fig. 3 — third panel). Three weaker components were observed around 36 (CM5), 41 (CM6), and 45 (CM7)ms. The field maps of these components showed a dipolar pattern over the contralaterally stimulated somatosensory area, with some components forming pairs with opposite polarities. For example, the polarity of components CM2 and CM5 was opposite to the polarity of components CM1 and CM4.

In the high-band, the MEG signal (butterfly plot) exhibited clear peaks only at very early latencies with center peak at 19 ms (CH1) (Fig. 3 — last panel). For latency details see Table 1.

Fig. 4A represents the virtual channel's SEFs, its SNR and ITS for the whole-band, and Fig. 4B for the other three frequency bands. The filtering of MEG signals at different frequencies

was proved quite effective for improving the SNR and revealing the most responsive band for each component. The virtual channel SNR was improved from ~5 to ~7 after filtering in the medium-band (Fig. 4C). The SNR of the virtual channel was quite low for the low-band at short-latency responses, although a peak with value around 2 could be seen in the SNR between 20 and 25 ms (first arrow in top part Fig. 4B). These properties of the SEFs and the virtual channels are likely to be the result of high variability in the responses and/or weakened strength for generators with transient time course and power in higher frequencies eliminated by the low pass filtering at 50 Hz. For this frequency band, the strongest response (SNR~10) was observed at late latencies (around 80 ms) (second arrow in top part Fig. 4B). The most responsive frequency band for the short-latencies presenting the highest SNR was the medium-band. The SNR of the virtual channel for this frequency band was ~7 at around 20 ms after the stimulus onset. It presented three peaks (marked by arrows in the middle part of Fig. 4B) one at around 16 ms, one at around 20 ms, and one at around 25 ms. For the high-band, the virtual sensor analysis showed higher activity at short-latencies with only a relatively broad peak of SNR that reached the value 1 at 20 ms (Fig. 4B).

Source localisation for the whole-band (0–250 Hz)

The ECD analysis revealed one focal source at the peak of the N20 component for all subjects, which was located cytoarchitectonically in contralateral area 3b (Fig. 5). The MNI coordinates of these fits and the corresponding probabilities for the BA3b are provided in Table 2 for the left wrist stimulation. GOF was >90% for all runs except one. The localisation results were consistent among runs (see Fig. 5 for left wrist stimulation); the averaged difference in source localisation between runs was 4.84±2.43 mm for the left and 5.32±3.28 mm for the right wrist stimulation at 20.8 ms by excluding the only run (subject 3 run 2) with GOF <90%. Variations between runs may be due to ambient field noise or brain activity that is not precisely time-locked to the stimulation, or change considerably across time, e.g. because of habituation. Monte-Carlo simulations revealed that the confidence volume of the ECD fits at the peak of N20 lay mostly on the BA3b and not on the BA4 (see Fig. 6). The overlap between the ECD localisation confidence regions and the representation of BA3b in the cytoarchitectonic maximum probability maps was found to be 63% while for BA4p and BA4a were 12% and 17%, respectively (all subjects, all runs).

In four subjects, GOF was >90% at 24.8 ms and 28.8 ms, and in three subjects at ~35 ms. In half of our subjects, a specific localisation pattern was observed for the time-points around 20 ms after stimulus onset, as shown for one representative subject in Fig. 7: the ECD started to approach the contralateral BA3b ~18 ms after the stimulus onset. It reached the ‘heart’ of BA3b at the peak of N20 component around 21 ms (upper panel of Fig. 7) with probabilities higher than 60% (mean probability: 73.3% for left wrist stimulation, 68.3% for right wrist stimulation). The ECD solution then moved from BA3b and approached the ‘center’ of BA2 (lower panel of Fig. 7) (mean probability: 68.3% for left wrist stimulation, 61.6% for right wrist stimulation), and at later latencies the BA1 (Fig. 8) (mean probability: 65% for left and for right wrist stimulation). However, the GOF was higher than 90% only at few time-points, and thus only for these time-points the localisation of single ECD could be considered reliable (Fig. 8).

MFT on averages revealed a similar localisation pattern with ECD. One peak in the MFT solutions was located at the contralateral postcentral gyrus in all subjects. It started to be active at around 16–17 ms. At this early latency, it was located in BA3b (mean probability: 62.2%), while later it was spread to BA4, BA1, and BA2. The activity was strongest at the peak of N20 component around 21 ms for all subjects. In accordance with the ECD analysis findings, MFT solutions had peaks few milliseconds later in BA2 (mean probability: 57.4%) and BA1 (mean probability: 58.8%).

Source localisation for the low-band (0–50 Hz)

The SNR of MEG signal was not high enough to provide dipole fits with GOF >90% at early latencies. ECDs at the peak of component around 35 ms were localised in BA1 in four subjects, though their GOF was low and thus these localisation results cannot be considered reliable. MFT revealed a weak generator located in BA3b at around 20 ms after stimuli onset, and another weak generator in BA1 around 35 ms for three subjects.

Source localisation for the medium-band (50–150 Hz)

More details are provided for the localisation results of this frequency band, since it showed the highest SNR for the short-latency range. The ECD analysis produced slightly higher GOF values compared to the whole frequency band (see Table 2) and much higher compared to the other two bands (low and medium) at the peak of N20. For this latency and averaged over both runs, the GOF was improved from 93.8% to 96.1% by filtering the data in the medium-band for the left wrist stimulation, and from 91.6% to 95.3% for the right wrist stimulation. In five out of six subjects, the GOF was >90% from 20 to 24 ms, and 26.4 to 30.4 ms (Fig. 9). In two subjects, the GOF was also >90% around 16 and around 35 ms. As one would expect, the ECD location did not localise to any specific cytoarchitectonic area for the latencies with low GOF. However, as the peak of N20 was approached and the GOF increased the dipole position localised to area BA3b (see Fig. 9, mean probability: 70.83% ±11.64 for all subjects — both hemispheres). The MNI coordinates of the ECD fits and the corresponding probabilities for the BA3b are provided in Table 2 for the left wrist stimulation. Two milliseconds later the ECD approached BA1 (mean probability: 78.33% ±11.69 for three of the subjects — both hemispheres), and it was moved out of SI 1–2 ms later Fig. 9). At around 28–29 ms, the ECD approached BA3b again (mean probability: 63.33%±12.30 for the same three subjects — both hemispheres) and 1–2 ms later BA1 (mean probability: 71.66%±7.52 for the three subjects — both hemispheres). The ECD was located in contralateral BA3b at the peak of N20 in all subjects (both hemispheres). In three of the subjects, the sequence of activity (BA3b → BA1 → BA3b → BA1) from 20 to 30 ms was consistent and clearly identified in both the two runs and the two hemispheres. The sequence (BA3b → BA1 → BA3b → BA1) was not clearly evident in the ECD solutions of the other three subjects, very likely because of more overlap in the activations of BA3b and BA1 and possibly simultaneous activity in other areas.

The MFT solutions of averaged data revealed a complex localisation pattern for this frequency band. The pattern was largely consistent across subjects with specific sequences of activations identified more clearly again in three of the six subjects. This sequence of activations is displayed in Fig. 10 for one of these subjects (same subject and hemisphere as

in Fig. 9). Only weak brain activations were identified at early latencies, the first one at 15–16 ms at BA3b. Later, between 16 and 19 ms, the activity was identified in a number of areas (in addition to the source in BA3b also in BA1 and possibly BA2 and BA4), often overlapping in time. From 19 to 22 ms, the activity was strong (with peak latency at 21.6 ms) with current density direction opposite to the one in the earlier period; this activity was focal and consistent in location with BA3b (mean probability for the three subjects: 67.8% ±8.32 at 21.6 ms). Between 22 and 25 ms the activity was attenuated and identified beyond BA3b, in BA1 (mean probability for the three subjects: 62.3%±9.52) and BA2 (mean probability for the three subjects: 60.8%±11.32), consistent with the findings of the ECD analysis. Between 26 and 28 ms, a strong activity was identified in BA3b becoming focal and reaching the overall maximum of the entire display period (15.2 to 30.4 ms) at 27.2 ms (mean probability for the three subjects: 63.6%±7.64). In the last part of the display period (28.8–30.4 ms), the BA3b generator attenuated as other sources were observed first in BA2 and a few ms later in BA1. For the rest three subjects, only a focal source in BA3b was revealed by MFT analysis at the peak of N20 component for both hemispheres (mean probability for all subjects: 64.2%±10.63). In summary, the MFT solutions were consistent with the ECD localisation when a single focal source was active; when MFT localised multiple sources for a specific time-point the ECD gave low GOF values and failed to localise these multiple sources. Five sources were localised by MFT: in BA3b, BA1, BA2, BA4a, and BA4p. The localisation findings of MFT analysis were consistent for both hemispheres with few exceptions.

Source localisation for the high-band (150–250 Hz)

The ECD analysis revealed GOF values >90% only in one time-point at the peak of N20 component (21.6 ms) for three out of six subjects. The localisation results were consistent among the subjects: ECDs were localised in BA3b with a probability of more than 80%. MFT revealed a weak generator located between BA1 and BA2 being active from 20 to 21.6 ms that peaks at 21.6 ms.

Discussion

Several studies have investigated the different properties of the ‘early’ cerebral responses elicited by median nerve electrical stimulation including the latency-amplitude, topographic distribution, and equivalent source location during selective stimulation of different body parts. Despite this, there are still considerable uncertainties as to which cortical areas are activated, or at least which of the areas activated by this type of stimulation can be unambiguously identified from non-invasive macroscopic measures like EEG and MEG. The traditional view posits that the main generator is located primarily in the posterior bank of the central sulcus, corresponding to BA3b (Inui et al., 2004; Mima et al., 1998; Tiihonen et al., 1989; Yang et al., 1993). An alternative view assumes a near simultaneous activation of an extended cortical region, which includes all subdivisions of SI (Papakostopoulos and Crow, 1980) and extends both anterior to the precentral gyrus (BA4) and posterior in the parietal lobe (Forss et al., 1994). Other weaker sources have also been reported to be active within the same short-latency range: ipsilateral SI (Korvenoja et al., 1995), contralateral SII (Karhu and Tesche, 1999), and cerebellum (Tesche and Karhu, 1997).

The conclusions about the generators of SEFs drawn in earlier studies were based on macroanatomical landmarks and analogies with activations identified during intraoperative recordings in humans undergoing neurosurgery (Allison et al., 1989), or direct recordings in animals (McCarthy et al., 1991). As commented earlier, inference on activated cortical areas drawn by comparison to the surrounding gyral and sulcal landmarks should be considered plausible suggestions, at best.

Invasive methods such as cortical surface, transcortical, and depth probe recordings are regarded as the gold standard for localising the generators of short-latency somatosensory responses. This is indeed the case provided certain conditions are satisfied: all aspects of the measurement are very precise; the local anatomy is not too distorted due to pathology; and histological analysis of the area is available. In practice, real invasive measurements in humans have clinical priorities with research needs having a minor significance and as a result they often fall far short in meeting the above criteria. For example, spatial resolution is limited because the inter-electrode spacing is usually ~5–6 mm for cortical surface recordings (Allison et al., 1989; Wood et al., 1988) and the measurements provide only a partial view in the strict locality where the needle has ended (i.e. in transcortical or depth probe recordings). In addition, expansive lesions in human patients may lead to functional reorganization altering the topographic organization of the cortex (Wunderlich et al., 1998; Vates et al., 2002). The methods used for localising the cortical generators are also biased towards clinical requirements that usually require a more macroscopic view, for example assessing the polarity and gradient of potentials recorded from the cortical surface and white matter. A polarity inversion and sharp potential gradient from surface to white matter are regarded as providing strong evidence that the potentials are generated in cortex between or adjacent to the recordings electrodes (Allison et al., 1991a; Wood et al., 1988). These limitations are minimized in invasive animal studies, but here evolutionary issues caution against confident generalization to humans.

Our methodology is a first step towards an attractive alternative based on direct reference to the cytoarchitectonic information in stereotaxic space given by the PCMs. It makes use of the MEG signal that is a direct macromeasure of the underlying neuronal activity — the signal reflects instantaneous changes in electrical activity and propagates from the point of generation in the brain to the sensors with the speed of light. The neuronal activity can be localised with an accuracy of 2–3 mm when strong enough and located in superficial sites such as during short-latency somatosensory responses.

The findings of the present study confirm the hypothesis that the earliest cortical response after median nerve stimulation (the early part of N20) is generated within the contralateral cytoarchitectonic area BA3b. Both inverse methods (ECD and MFT) identified a focal source within BA3b at the peak of N20 (with high PCM probability). The findings were consistent among subjects (see Fig. 5 for ECD) and the GOF was high for the ECD fits indicating reliable localisation fits. Our results are in full agreement with the findings from previous somatosensory evoked potential (SEP) and SEF studies (Inui et al., 2004; Wood et al., 1985) but also from intracranial findings in humans (Allison et al., 1989; 1991b) and monkeys (McCarthy et al., 1991). These studies concluded that short-latency cortical SEPs are generated primarily if not exclusively in areas 3b and 1. SEPs derived from cortical

surface in humans (Allison et al., 1991b) showed a polarity inversion from P20-N30 to N20-P30 across the posterior wall of the central sulcus indicating a focal generator located mainly in area 3b. SEP and multiunit recordings from Old World monkeys demonstrated that the P10 and N10 potentials (corresponding to the human P20 and N20) are generated in the anterior wall of the postcentral gyrus, which is comprised mainly of area 3b (McCarthy et al., 1991). Here, no strong activity was found for area 4 except weak sources detected and localised by MFT. Our Monte-Carlo analysis of average MEG signals suggests that the P20 in humans and (assuming homology) the corresponding potential P10 in monkeys are associated with strong unit discharges in area 3b but not in area 4 (see Fig. 6). This is in line with anatomical findings according to which somatosensory afferent projections of area 4 of motor cortex are sparse compared with those to area 3b (Jones and Powell, 1970). In both humans (Stohr and Goldring, 1969; Wood et al., 1986) and monkeys (Allison et al., 1986), surgical removal of the hand area of somatosensory cortex abolishes all median nerve SEPs, whereas lesions of motor cortex in monkeys were found to have little effect on P10-N20 and N10-P20 (Allison et al., 1986). Inline with this notion, surface and intracerebral recordings from the cortex and white matter of macaca precentral gyrus did not show sharp voltage gradients or polarity inversions indicative of locally generated activity (McCarthy et al., 1991; Gardner et al., 1984).

A second weaker source located probably in BA1 started to be active few milliseconds after the peak of N20 representing the P25 component that was more prominent in the medium-band, and detectable in four subjects. When the whole frequency band was analyzed, the ECD approached the ‘center’ of area 2 instead of 1. This inconsistency could be due to the relatively low SNR of this component at the whole frequency band (see Fig. 4) that was markedly increased by filtering the signal in the medium-band. The area 1 is located in the crown of the postcentral gyrus and it therefore corresponds to a nearly radial generator. Thus, it is to be expected that a weak MEG signal would be generated that is difficult to be detected. The activation of BA1 is in agreement with cortical surface and intraoperative recordings during neurosurgery and recordings from chronically implanted depth probes in epileptic patients (Allison et al., 1989). These studies found the P25 component as a distinct entity in 30% of the cases. Allison et al. (1989) reported its latency 3 ms after the N20 peak, corresponding to ~22 ms after stimulus onset. They found that the P25-N35 component was largest in the anteromedial portion of the hand area of somatosensory cortex, while its potential distribution suggested a radially oriented generator in area 1, which in humans and Old World monkeys is located primarily in the anterior crown of the postcentral gyrus (Powell and Mountcastle, 1959). In animals, the P12-N25 component (corresponding to the human P25-N35) has also been recorded over most of the crown of somatosensory cortex indicating a partial activation of area 1 and maybe area 2.

Our results support the notion of a serial mode of somatosensory processing through the postcentral gyrus from BA3b to BA1. The serial activation in areas 3b and 1 is also supported by previous MEG studies (Inui et al., 2004; Kakigi, 1994), intracranial SEP studies in monkeys (Allison et al., 1991b; Garraghty et al., 1990), and anatomical finding in monkeys according to which the area 3 projects predominantly into area 1 (Vogt and Pandya, 1978). The component C3 at ~30 ms seems to represent a second wave of reactivations of areas 3b and 1. This is clearer in the most responsive medium frequency band, where the

ECD fits have higher GOFs (see Fig. 9). Our results suggest that the positive and the negative phases of the P20-N30 component at ~20 and ~30 ms are actually generated by the same neural source. The same may also be for the positive and negative phases of the P25-N35 component peaking at ~25 and ~35 ms. This is in accordance with previous transcortical SEPs data which were well accounted for by a model having two generators with different time courses (shifted by ~5 ms) and with fixed locations and orientations in the BA3b and BA1 (Allison et al., 1989). These positive-negative sequences are often called the primary evoked responses (Towe, 1966) and have been recorded from visual, auditory, and somatosensory cortex (Mitzdorf, 1985; Schlag, 1973; Towe, 1966). Whether the reoccurrence of BA3b activity is a “second wave” or a feedback from the area 1 cannot be concluded by the findings of the present study.

The first cortical activation was observed firstly at around 15–16 ms (see Fig. 4) after stimulus onset. MFT and ECD localised this source in areas 3b and 1, with a hint of an earlier onset in BA3b. The rather low GOF (<90%) of the ECD solution (see Fig. 9) can be understood as a consequence of the relative weakness of this early activation, collaborated also by the relatively low source strength of the MFT solution (see Fig. 10). This early cortical activity is likely to overlap with activity in deep subcortical areas along thalamocortical fibers (Kimura et al., 2008), and this might be why it was not identified in some subjects.

Methodological issues

From a more methodological point of view, the results of both simulation and human data confirm the hypothesis outlined in the Introduction. The analysis of MEG data and the use of PCMs allow under preconditions (very high values of GOF for the single ECD model) unambiguous interpretation of cytoarchitectonic identity of activated areas following median nerve stimulation. In the present study, the measured brain activity was modeled using a single ECD at each time-point. Only ECD fittings with very high GOF were assumed reliable. In the other time-points where the GOF was low, the recorded magnetic activity could be attributed to many different generators simultaneously active or distributed over a significant brain area and thus the ECD model may perform poorly (Phillips et al., 1997). This was confirmed by MFT showing that more than one generator were active within SI.

According to the simulation data, the GOF is a good indicator of the reliability of the ECD solution. ECD solutions with very high GOF (above 96%) indicate that the MEG signal is dominated by either a single focal source, or a couple of sources within a few millimeters of each other. On the basis of our simulation data (Fig. 2), the ECD model reliably identifies the location of a single focal source (with an accuracy of ~1 mm and a GOF of>98%). These results are in full agreement with earlier MFT studies performed with data providing only partial head coverage (Ioannides et al., 1993a,b) and more recent studies with realistically head-shaped phantoms (Papadelis et al., 2007,2009). The results from the present study show that the overlay of functional solutions of high GOF on the PCMs can provide unambiguous identification of the active cytoarchitectonic area. When more than one source was simultaneously active and almost equally strong, the GOF was decreased below ~96% indicating that a single ECD model is not an appropriate description of the measured

activity. In summary we find that, ECD solutions with GOF >95% are necessary for the corresponding location to be close enough to a true source and thus allow histological allocation by the PCMs. This is particularly evident for the ECD results in the most responsive medium-band. Periods with high GOF and assignment with high probability to one or other cytoarchitectonic area were interspersed between periods with low GOF and the ECD "wandering" in the space in between well-defined cytoarchitectonic areas. During periods of ECD solutions with high GOF, the MFT analysis showed focal activity in the same cytoarchitectonic areas as the ECD. In the other periods, when the GOF of the ECD solutions was low, MFT showed activity of similar magnitude in different areas (some captured in the slices displayed in Fig. 10). A multiple dipole approach may provide even more accurate localisation results when multiple generators are simultaneously active, a topic that is now under further investigation in our laboratories.

Our results also showed that filtering can determine what history emerges from the ECD analysis. By definition, low frequency filtering will only allow through slow components, so each one of the brief early activations will be largely eliminated, or at least greatly reduced and spread so the identity of each source will be lost as their signals overlap with each other. It is therefore not surprising that the low frequency analysis did not produce well-differentiated early focal activations. The high-frequency range of 150 to 250 Hz leads to ECD solutions only close to the peak of the N20, suggesting that the activity at the other latencies contained significant power at the eliminated lower frequencies below 150 Hz. Our results suggest that for transitions within and close to SI for the early responses the frequency range from 50 to 150 Hz provides the best view of the early interchanges of activity between areas.

Conclusions

In summary, we have demonstrated that the earliest responses are generated in area 3b and provided evidence for serial processing within cytoarchitectonic SI subdivisions. Using the well-established ECD analysis we could account for the major spatial and temporal features of SEFs in the most responsive frequency band (medium-band of 50–150 Hz) with a model having two main generators with slightly different time courses one in cytoarchitectonic area 3b and the other in area 1. A possible contribution from other sources cannot be ruled out and MFT analysis produced some evidence for activity in areas 2, 4a and 4p. These results show that ECD analysis of MEG data are reliable enough to determine which cytoarchitectonic area is activated on the basis of PCMs, but only at latencies where the solutions have very high GOF, at least 95% but better still above 97%. Under these conditions the MEG measurements and their simple ECD analysis offer a non-invasive and easy to use tool to localise the underlying neural generators of SEFs.

Acknowledgments

We thank all the staff of the Laboratory for Human Brain Dynamics (1999–2009) at the Brain Science Institute, RIKEN and especially Mr. Kenji Haruhana for the assistance with the experiment. The experiment and data analysis were performed at RIKEN and the work was continued by the authors at their new posts in Italy and Cyprus. Following the closing of the MEG laboratory at RIKEN in September 2009, the contribution from AAI was supported by Cyprus Research Promotion Foundation grants (upgrade/info/0308/02 and human/sociol/0308/BE).

SBE was supported by the Human Brain Project (R01-MH074457-01A1), and SBE and KZ by the Helmholtz Initiative on Systems Biology “The Human Brain Model”.

Abbreviations:

BA1	Brodmann area 1
BA3b	Brodmann area 3b
ECD	Equivalent current dipole
ECG	Electrocardiogram
EEG	Electroencephalography
EOG	Electrooculogram
fMRI	Functional magnetic resonance imaging
GOF	Goodness of fit
ICA	Independent component analysis
ITS	Intertrial synchronization index
LE	Localisation error
MEG	Magnetoencephalography
MFT	Magnetic field tomography
MNI	Montreal Neurological Institute
MTH	Motor threshold
PCMs	Probabilistic cytoarchitectonic maps
PET	Positron emission tomography
S1	Primary somatosensory area
SEF	Somatosensory evoked field
SEP	Somatosensory evoked potential
SNR	Signal-noise-ratio
ST	Single trial
STH	Sensory threshold
V1	Primary visual area

References

Allison T, Wood CC, McCarthy G, 1986. Somatosensory evoked potentials following surgical excision of somatosensory or motor cortex in the monkey. Soc. Neurosci. Abstr. 12,1432.

Allison T, McCarthy G, Wood CC,Jones SJ, 1991a. Potentials evoked in human and monkey cerebral cortex by stimulation of the median nerve. A review of scalp and intracranial recordings. Brain 114 (Pt 6), 2465–2503. [PubMed: 1782527]

Allison T, Wood CC, McCarthy G, Spencer DD, 1991b. Cortical somatosensory evoked potentials. II. Effects of excision of somatosensory or motor cortex in humans and monkeys. J. Neurophysiol. 66 (1), 64–82. [PubMed: 1919677]

Allison T, McCarthy G, Wood CC, Darcey TM, Spencer DD, Williamson PD, 1989. Human cortical potentials evoked by stimulation of the median nerve. I. Cytoarchitectonic areas generating short-latency activity. J. Neurophysiol. 62 (3), 694–710. [PubMed: 2769354]

Amiez C, Petrides M, 2009. Anatomical organization of the eye fields in the human and non-human primate frontal cortex. Progr. Neurobiol. 89, 220–230.

Amunts K, Schleicher A, Bürgel U, Mohlberg H, Uylings HBM, Zilles K, 1999. Broca's region revisited: cytoarchitecture and intersubject variability. J. Comp. Neurol. 412,319–341. [PubMed: 10441759]

Amunts K, Malikovic A, Mohlberg H, Schormann T, Zilles K, 2000. Brodmann's areas 17 and 18 brought into stereotaxic space — where and how variable? Neuroimage 11, 66–84. [PubMed: 10686118]

Amunts K, Zilles K, 2001. Advances in cytoarchitectonic mapping of the human cerebral cortex. Neuroimaging Clin. N. Am. 11 (2), 151–169. [PubMed: 11489732]

Amunts K, Weiss PH, Mohlberg H, Pieperhoff P, Eickhoff S, Gurd JM, Marshall JC, Shah JN, Fink GR, Zilles K, 2004. Analysis of the neural mechanisms underlying verbal fluency in cytoarchitectonically defined stereotaxic space — the roles of Brodmann areas 44 and 45. Neuroimage 22, 42–56. [PubMed: 15109996]

Ashburner J, Friston KJ, 2005. Unified segmentation. Neuroimage 26 (3), 839–851. [PubMed: 15955494]

Barnikol UB, Amunts K, Dammers J, Mohlberg H, Fieseler T, Malikovic A, Zilles K, Niedeggen M, Tass PA, 2006. Pattern reversal visual evoked responses of V1/V2 and V5/MT as revealed by MEG combined with probabilistic cytoarchitectonic maps. Neuroimage 31 (1), 86–108. [PubMed: 16480895]

Baumgartner C, Sutherling WW, Di S, Barth DS, 1991. Spatiotemporal modeling of cerebral evoked magnetic fields to median nerve stimulation. Electroencephalogr. Clin. Neurophysiol. 79 (1), 27–35. [PubMed: 1713549]

Binkofski F, Amunts K, Stephan KM, Posse S, Schormann T, Freund HJ, Zilles K, Seitz RJ, 2000. Broca's region subserves imagery of motion: a combined cytoarchitectonic and fMRI study. Hum. Brain Mapp. 11 (4), 273–285. [PubMed: 11144756]

Bodegård A, Geyer S, Naito E, Zilles K, Roland PE, 2000. Somatosensory areas in man activated by moving stimuli. Cytoarchitectonic mapping and PET. NeuroReport 11, 187–191. [PubMed: 10683855]

Bodegård A, Geyer S, Herath P, Grefkes C, Zilles K, Roland PE, 2003. Somatosensory areas engaged during discrimination of steady pressure, spring strength and kinaesthesia. Hum. Brain Mapp. 20,103–115. [PubMed: 14505336]

Brodmann K, 1909. Vergleichende Lokalisationslehre der Großhirnrinde. Barth, Leipzig.

Buchner H, Fuchs M, Wischmann HA, Dössel O, Ludwig I, Knepper A, Berg P, 1994. Source analysis of median nerve and finger stimulated somatosensory evoked potentials: multichannel simultaneous recording of electric and magnetic fields combined with 3D-MR tomography. Brain Topogr. 6 (4), 299–310. [PubMed: 7946929]

Dammers J, Mohlberg H, Boers F, Tass P, Amunts K, Mathiak K, 2007. A new toolbox for combining magnetoencephalographic source analysis and cytoarchitectonic probabilistic data for anatomical classification of dynamic brain activity. Neuroimage 34, 1577–1587. [PubMed: 17187996]

Dumoulin SO, Bittar RG, Kabani NJ, Baker CL Jr., Le Goualher G, Bruce Pike G, Evans AC, 2000. A new anatomical landmark for reliable identification of human area V5/MT: a quantitative analysis of sulcal patterning. Cereb. Cortex 10 (5), 454–463. [PubMed: 10847595]

Eickhoff SB, Stephan KE, Mohlberg H, Grefkes C, Fink GR, Amunts K, Zilles K, 2005. A new SPM toolbox for combining probabilistic cytoarchitectonic maps and functional imaging data. Neuroimage 25 (4), 1325–1335. [PubMed: 15850749]

Eickhoff SB, Heim S, Zilles K, Amunts K, 2006a. Testing anatomically specified hypotheses in functional imaging using cytoarchitectonic maps. Neuroimage 32 (2), 570–582. [PubMed: 16781166]

Eickhoff SB, Lotze M, Wietek B, Amunts K, Enck P, Zilles K, 2006b. Segregation of visceral and somatosensory afferents: an fMRI and cytoarchitectonic mapping study. Neuroimage 31 (3), 1004–1014. [PubMed: 16529950]

Eickhoff SB, Paus T, Caspers S, Grosbras MH, Evans A, Zilles K, Amunts K, 2007. Assignment of functional activations to probabilistic cytoarchitectonic areas revisited. Neuroimage 36 (3), 511–521. [PubMed: 17499520]

Eickhoff SB, Grefkes C, Fink GR, Zilles K, 2008. Functional lateralisation of face, hand and trunk representation in anatomically defined human somatosensory areas. Cereb. Cortex 18, 2820–2830. [PubMed: 18372289]

Evans AC, Marrett S, Neelin P, Collins L, Worsley K, Dai W, Milot S, Meyer E, Bub D, 1992. Anatomical mapping of functional activation in stereotactic coordinate space. Neuroimage 1, 43–53. [PubMed: 9343556]

Forss N, Hari R, Salmelin R, Ahonen A, Hämäläinen M, Kajola M, Knuutila J, Simola J, 1994. Activation of the human posterior parietal cortex by median nerve stimulation. Exp. Brain Res. 99 (2), 309–315. [PubMed: 7925811]

Gardner EP, Hämäläinen HA, Warren S, Davis J, Young W, 1984. Somatosensory evoked potentials (SEPs) and cortical single unit response elicited by mechanical tactile stimuli in awake monkeys. Electroencephalogr. Clin. Neurophysiol. 58,537–552. [PubMed: 6209104]

Garraghty PE, Florence SL, Kaas JH, 1990. Ablations of areas 3a and 3b of monkey somatosensory cortex abolish cutaneous responsivity in area 1. Brain Res. 528 (1), 165–169. [PubMed: 2245335]

Geyer S, Ledberg A, Schleicher A, Kinomura S, Schormann T, Burgel U, Klingberg T, Larsson J, Zilles K, Roland PE, 1996. Two different areas within the primary motor cortex of man. Nature 382, 805–807. [PubMed: 8752272]

Geyer S, Schleicher A, Zilles K, 1999. Areas 3a, 3b, and 1 of human primary somatosensory cortex: 1. Microstructural organization and interindividual variability. Neuroimage 10, 63–83. [PubMed: 10385582]

Geyer S, Schormann T, Mohlberg H, Zilles K, 2000. Areas 3a, 3b, and 1 of human primary somatosensory cortex. 2. Spatial normalization to standard anatomical space. Neuroimage 11, 684–696. [PubMed: 10860796]

Geyer S, Schleicher A, Schormann T, Mohlberg H, Bodegard A, Roland PE, Zilles K, 2001. Integration of microstructural and functional aspects of human somatosensory areas 3a, 3b, and 1 on the basis of a computerized brain atlas. Anat. Embryol. (Berl) 204 (4), 351–366. [PubMed: 11720238]

Grefkes C, Geyer S, Schormann T, Roland P, Zilles K, 2001. Human somatosensory area 2: observer-independent cytoarchitectonic mapping, interindividual variability, and population map. Neuroimage 14,617–631. [PubMed: 11506535]

Gross J, Ioannides AA, 1999. Linear transformations of data space in MEG. Phys. Med. Biol. 44, 2081–2097. [PubMed: 10473216]

Hämäläinen M, Hari R, Ilmoniemi RJ, Knuutila J, Lounasmaa OV, 1993. Magnetoencephalography — theory, instrumentation, and applications to noninvasive studies of the working human brain. Rev. Mod. Phys. 65 (2), 413–497.

Hari R, Reinikainen K, Kaukoranta E, Hämäläinen M, Ilmoniemi R, Penttinen A, Salminen J, Teszner D, 1984. Somatosensory evoked cerebral magnetic fields from SI and SII in man. Electroencephalogr. Clin. Neurophysiol. 57 (3), 254–263. [PubMed: 6199186]

Haueisen J, Schack B, Meier T, Curio G, Okada Y, 2001. Multiplicity in the high-frequency signals during the short-latency somatosensory evoked cortical activity in humans. Clin. Neurophysiol. 112 (7), 1316–1325. [PubMed: 11516744]

Heim S, Alter K, Ischebeck AK, Amunts K, Eickhoff SB, Mohlberg H, Zilles K, Yves von Cramon D, Friederici AD, 2005. The role of the left Brodmann's areas 44 and 45 in reading words and pseudowords. Cognit. Brain Res. 25, 982–993.

Hironaga N, Ioannides AA, 2002. Accurate co-registration for MEG reconstructions. In: Nowak H, Haueisen J, Giessler F, Huonker R (Eds.), Proceedings of the 13th International Conference on Biomagnetism. Berlin, VDE Verlag, pp. 931–933.

Horwitz B, Amunts K, Bhattarchayya R, Patkin D, Jeffries K, Zilles K, Braun AR, 2003. Activation of Broca's area during the production of spoken and signed language: A combined cytoarchitectonic mapping and PET analysis. Neuropsychologia 41, 1868–1876. [PubMed: 14572520]

Huttunen J, 1997. Does the P35m SEF deflection really come from the motor cortex? Electroencephalogr. Clin. Neurophysiol. 104 (1), 101–102. [PubMed: 9076260]

Ioannides AA, 1995. Estimates of 3D brain activity ms by ms from biomagnetic signals: method (MFT), results and their significance. In: Eiselt E, Zwiener U, Witte H (Eds.), Quantitative and Topological EEG and MEG analysis. Universitatsverlag Druckhaus-Maayer GmbH, Jena, pp. 59–68.

Ioannides AA, 2006. Magnetoencephalography as a research tool in neuroscience: State of the art. Neuroscientist 12, 524–544. [PubMed: 17079518]

Ioannides AA, Bolton JPR, Clarke CJS, 1990. Continuous probabilistic solutions to the biomagnetic inverse problem. Inverse problem 6, 523–542.

Ioannides AA, Hellstrand E, Abraham-Fuchs K, 1993a. Point and distributed current density analysis of interictal epileptic activity recorded by magnetoencephalography. Physiol. Meas. 14,121–130. [PubMed: 8334407]

Ioannides AA, Singh KD, Hasson R, Baumann SB, Rogers RL, Guinto FC, Papanicolaou AC, 1993b. Comparison of current dipole and magnetic field tomography analyses of the cortical response to auditory stimuli. Brain Topogr. 6, 27–34. [PubMed: 8260323]

Ioannides AA, Kostopoulos GK, Laskaris NA, Liu LC, Shibata T, Schellens M, Poghosyan V, Khurshudyan A, 2002. Timing and connectivity in the human somatosensory cortex from single trial mass electrical activity. Hum. Brain Mapp. 15, 231–246. [PubMed: 11835611]

Inui K, Wang X, Tamura Y, Kaneoke Y, Kakigi R, 2004. Serial processing in the human somatosensory system. Cereb. Cortex 14 (8), 851–857. [PubMed: 15054058]

Jakobs O, Wang LE, Dafotakis M, Grefkes C, Zilles K, Eickhoff SB, 2009. Effects of timing and movement uncertainty implicate the temporo-parietal junction in the prediction of forthcoming motor actions. Neuroimage 47 (2), 667–677. [PubMed: 19398017]

Jones EG, Powell TPS, 1970. Connexions of the somatic sensory cortex of the rhesus monkey. III. Thalamic connexions. Brain 93, 37–56. [PubMed: 4984909]

Kakigi R, 1994. Somatosensory evoked magnetic fields following median nerve stimulation. Neurosci. Res. 20 (2), 165–174. [PubMed: 7808699]

Karhu J, Tesche CD, 1999. Simultaneous early processing of sensory input in human primary (SI) and secondary (SII) somatosensory cortices. J. Neurophysiol. 81 (5), 2017–2025. [PubMed: 10322043]

Kawamura T, Nakasato N, Seki K, Kanno A, Fujita S, Fujiwara S, Yoshimoto T, 1996. Neuromagnetic evidence of pre- and post-central cortical sources of somatosensory evoked responses. Electroencephalogr. Clin. Neurophysiol. 100 (1),44–50. [PubMed: 8964262]

Kimura T, Ozaki I, Hashimoto I, 2008. Impulse propagation along thalamocortical fibers can be detected magnetically outside the human brain. J. Neurosci. 28 (47), 12535–12538. [PubMed: 19020045]

Korvenoja A, Wikstrom H, Huttunen J, Virtanan J, Laine P, Aronen HJ, Seppalainen AM, Ilmoniemi RJ, 1995. Activation of ipsilateral primary sensorimotor cortex by median nerve stimulation. NeuroReport 6 (18), 2589–2593. [PubMed: 8741769]

Laskaris NA, Ioannides AA, 2001. Exploratory data analysis of evoked response single trials based on minimal spanning tree. Clin. Neurophysiol. 112 (4), 698–712. [PubMed: 11275544]

Laskaris NA, Liu LC, Ioannides AA, 2003. Single-trial variability in early visual neuromagnetic responses: an explorative study based on the regional activation contributing to the N70m peak. Neuroimage 20 (2), 765–783. [PubMed: 14568450]

Leahy RM, Mosher JC, Spencer ME, Huang MX, Lewine JD, 1998. A study of dipole localization accuracy for MEG and EEG using a human skull phantom. Electroencephalogr. Clin. Neurophysiol. 107 (2), 159–173. [PubMed: 9751287]

Lee TW, Girolami M, Sejnowski TJ, 1999. Independent component analysis using an extended INFOMAX algorithm for mixed sub-Gaussian and super-Gaussian sources. Neural Comput. 11, 606–633.

Liu LC, Ioannides AA, Mueller-Gaertner HW, 1998. Bi-hemispheric study of single trial MEG signals of the human auditory cortex. Electroenceph. Clin. Neurophysiol 106, 64–78. [PubMed: 9680166]

Mauguière F, Merlet I, Forss N, Vanni S, Jousmäki V, Adeleine P, Hari R, 1997. Activation of a distributed somatosensory cortical network in the human brain. A dipole modelling study of magnetic fields evoked by median nerve stimulation. Part I: Location and activation timing of SEF sources. Electroencephalogr. Clin. Neurophysiol. 104 (4), 281–289. [PubMed: 9246065]

McCarthy G, Wood CC, Allison T, 1991. Cortical somatosensory evoked potentials. I. Recordings in the monkey *Macaca fascicularis*. J. Neurophysiol. 66 (1), 53–63. [PubMed: 1919676]

Mima T, Nagamine T, Nishitani N, Mikuni N, Ikeda A, Fukuyama H, Takigawa T, Kimura J, Shibasaki H, 1998. Cortical myoclonus: sensorimotor hyperexcitability. Neurology 50 (4), 933–942. [PubMed: 9566375]

Mitzdorf U, 1985. Current source-density method and application in cat cerebral cortex: investigation of evoked potentials and EEG phenomena. Physiol. Rev. 65, 37–100. [PubMed: 3880898]

Mohlberg H, Lerch J, Amunts K, Evans AC, Zilles K, 2003. Probabilistic cytoarchitectonic maps transformed into MNI space. 9th International Conference on Functional Mapping of the Human Brain, June 19–22, 2003, New York. : NeuroImage, 19(2). Academic Press, San Diego.

Moradi F, Liu LC, Cheng K, Waggoner RA, Tanaka K, Ioannides AA, 2003. Consistent and precise localization of brain activity in human primary visual cortex by MEG and fMRI. Neuroimage 18 (3), 595–609. [PubMed: 12667837]

Papadelis C, Poghosyan V, Fenwick PB, Ioannides AA, 2009. MEG's ability to localise accurately weak transient neural sources. Clin. Neurophysiol. 120 (11), 1958–1970. [PubMed: 19782641]

Papadelis C, Poghosyan V, Ioannides AA, 2007. Phantom study supports claim of accurate localization from MEG data. Int. J. Bioelectromagnetism 9 (3), 163–167.

Papakostopoulos D, Crow HJ, 1980. Direct recording of the somatosensory evoked potentials from the cerebral cortex of man and the difference between precentral and postcentral potentials. In: Desmedt JE (Ed.), Clinical Uses of Cerebral, Brainstem and Spinal Somatosensory Evoked Potentials. : Progr Clin Neurophysiol, vol. 7. Basel, Karger, pp. 15–26.

Phillips JW, Leahy RM, Mosher JC, 1997. MEG-based imaging of focal neuronal current sources. IEEE Trans. Med. Imaging 16, 338–348. [PubMed: 9184896]

Poghosyan V, Ioannides AA, 2008. Attention modulates earliest responses in the primary auditory and visual cortices. Neuron 58, 802–813. [PubMed: 18549790]

Powell TPS, Mountcastle VB, 1959. The cytoarchitecture of the postcentral gyrus of the monkey *Macaca mulatta*. Bull. Johns Hopkins Hosp. 105,108–131. [PubMed: 14434572]

Prieto EA, Barnikol UB, Soler EP, Dolan K, Hesselmann G, Mohlberg H, Amunts K, Zilles K, Niedeggen M, Tass PA, 2007. Timing of V1/V2 and V5+ activations during coherent motion of dots: an MEG study. Neuroimage 37 (4), 1384–1395. [PubMed: 17689986]

Rossini PM, Deuschl G, Pizzella V, Tecchio F, Pasquarelli A, Feifel E, Romani GL, Lücking CH, 1996. Topography and sources of electromagnetic cerebral responses to electrical and air-puff stimulation of the hand. Electroencephalogr. Clin. Neurophysiol. 100 (3), 229–239. [PubMed: 8681864]

Schlag J, 1973. Generation of brain evoked potentials. In: Thompson RF, Patterson MM (Eds.), Bioelectric Recording Techniques: Cellular Processes and Brain Potentials, New York: Academic, part. A, pp. 273–316.

Schleicher A, Palomero-Gallagher N, Morosan P, Eickhoff SB, Kowalski T, de Vos K, Amunts K, Zilles K, 2005. Quantitative architectural analysis: a new approach to cortical mapping. Anat. Embryol. (Berl) 210 (5–6), 373–386. [PubMed: 16249867]

Stohr PE, Goldring S, 1969. Origin of somatosensory evoked scalp responses in man. J. Neurosurg. 31, 117–127. [PubMed: 5803802]

Taylor JG, Ioannides AA, Muller-Gartner HW, 1999. Mathematical analysis of lead field expansions. IEEE Trans. Med. Imaging 18,151–163. [PubMed: 10232672]

Tecchio F, Pasqualetti P, Pizzella V, Romani G, Rossini PM, 2000. Morphology of somatosensory evoked fields: inter-hemispheric similarity as a parameter for physiological and pathological neural connectivity. Neurosci. Lett. 287 (3), 203–206. [PubMed: 10863030]

Tecchio F, Rossini PM, Pizzella V, Cassetta E, Romani GL, 1997. Spatial properties and interhemispheric differences of the sensory hand cortical representation: a neuromagnetic study. Brain Res. 767 (1), 100–108. [PubMed: 9365021]

Tesche CD, Karhu J, 1997. Somatosensory evoked magnetic fields arising from sources in the human cerebellum. Brain Res. 744 (1), 23–31. [PubMed: 9030409]

Tiihonen J, Hari R, Hämäläinen M, 1989. Early deflections of cerebral magnetic responses to median nerve stimulation. Electroencephalogr. Clin. Neurophysiol. 74 (4), 290–296. [PubMed: 2471630]

Tootell RB, Reppas JB, Kwong KK, Malach R, Born RT, Brady TJ, Rosen BR, Belliveau JW, 1995. Functional analysis of human MT and related visual cortical areas using magnetic resonance imaging. J. Neurosci. 15 (4), 3215–3230. [PubMed: 7722658]

Towe AL, 1966. On the nature of the primary evoked response. Exp. Neurol. 15,113–139. [PubMed: 5934659]

Vates GE, Lawton MT, Wilson CB, McDermott MW, Halbach VV, Roberts TP, Rowley HA, 2002. Magnetic source imaging demonstrates altered cortical distribution of function in patients with arteriovenous malformations. Neurosurgery 51 (3), 614–623. [PubMed: 12188939]

Vogt BA, Pandya DN, 1978. Cortico-cortical connections of somatic sensory cortex (areas 3, 1 and 2) in the rhesus monkey. J. Comp. Neurol. 177 (2), 179–191. [PubMed: 413844]

Wikström H, Huttunen J, Korvenoja A, Virtanen J, Salonen O, Aronen H, Ilmoniemi RJ, 1996. Effects of interstimulus interval on somatosensory evoked magnetic fields (SEFs): a hypothesis concerning SEF generation at the primary sensorimotor cortex. Electroencephalogr. Clin. Neurophysiol. 100 (6), 479–487. [PubMed: 8980411]

Wilms M, Eickhoff SB, Specht K, Amunts K, Shah NJ, Malikovic A, Fink GR, 2005. Human V5/MT +: comparison of functional and cytoarchitectonic data. Anat. Embryol. (Berl) 210, 485–495. [PubMed: 16328357]

Wilms M, Eickhoff SB, Hömke L, Rottschy C, Kujovic M, Amunts K, Fink GR, 2010. Comparison of functional and cytoarchitectonic maps of human visual areas V1, V2, V3d, V3v, and V4(v). Neuroimage 49 (2), 1171–1179. [PubMed: 19800409]

Wohlschläger AM, Specht K, Lie C-H, Mohlberg H, Wohlschläger A, Bente K, Pietrzyk U, Stöcker T, Zilles K, Amunts K, Fink GR, 2005. Linking retinotopic fMRI mapping and anatomical probability maps of human occipital areas V1 and V2. Neuroimage 26, 73–82. [PubMed: 15862207]

Wood CC, Cohen D, Cuffin BN, Yarita M, Allison T, 1985. Electrical sources in human somatosensory cortex: identification by combined magnetic and potential recordings. Science 227 (4690), 1051–1053. [PubMed: 3975600]

Wood CC, Allison T, McCarthy G, Spencer DD, Williamson PD, 1986. Somatosensory evoked potentials following surgical excision of human somatosensory or motor cortex. Soc. Neurosci. Abstr. 12,1432.

Wood CC, Spencer DD, Allison T, McCarthy G, Williamson PD, Goff WR, 1988. Localization of human sensorimotor cortex during surgery by cortical surface recording of somatosensory evoked potentials. J. Neurosurg. 68 (1), 99–111. [PubMed: 3275756]

Wunderlich G, Knorr U, Herzog H, Kiwit JC, Freund HJ, Seitz RJ, 1998. Precentral glioma location determines the displacement of cortical hand representation. Neurosurgery 42 (1), 18–26. [PubMed: 9442499]

Yang TT, Gallen CC, Schwartz BJ, Bloom FE, 1993. Noninvasive somatosensory homunculus mapping in humans by using a large-array biomagnetometer. Proc. Natl Acad. Sci. 90 (7), 3098–3102. [PubMed: 8464929]

Young JP, Geyer S, Grefkes C, Amunts K, Morosan P, Zilles K, Roland PE, 2003. Regional cerebral blood flow correlations of somatosensory areas 3a, 3b, 1, and 2 in humans during rest: A PET and cytoarchitectural study. Hum. Brain Mapp. 19,183–196. [PubMed: 12811734]

Zeki S, Watson JD, Lueck CJ, Friston KJ, Kennard C, Frackowiak RS, 1991. A direct demonstration of functional specialization in human visual cortex. J. Neurosci. 11 (3), 641–649. [PubMed: 2002358]

Zilles K, Schleicher A, Palomero-Gallagher N, Amunts K, 2002. Quantitative analysis of cyto- and receptor architecture of the human brain. In: Mazziotta J, Toga A (Eds.), Brain Mapping, the Methods, Elsevier, pp. 573–602.

Zilles K, Amunts K, 2010. Centenary of Brodmann's map — conception and fate. Nat. Rev. Neurosci. 11 (2), 139–145. [PubMed: 20046193]

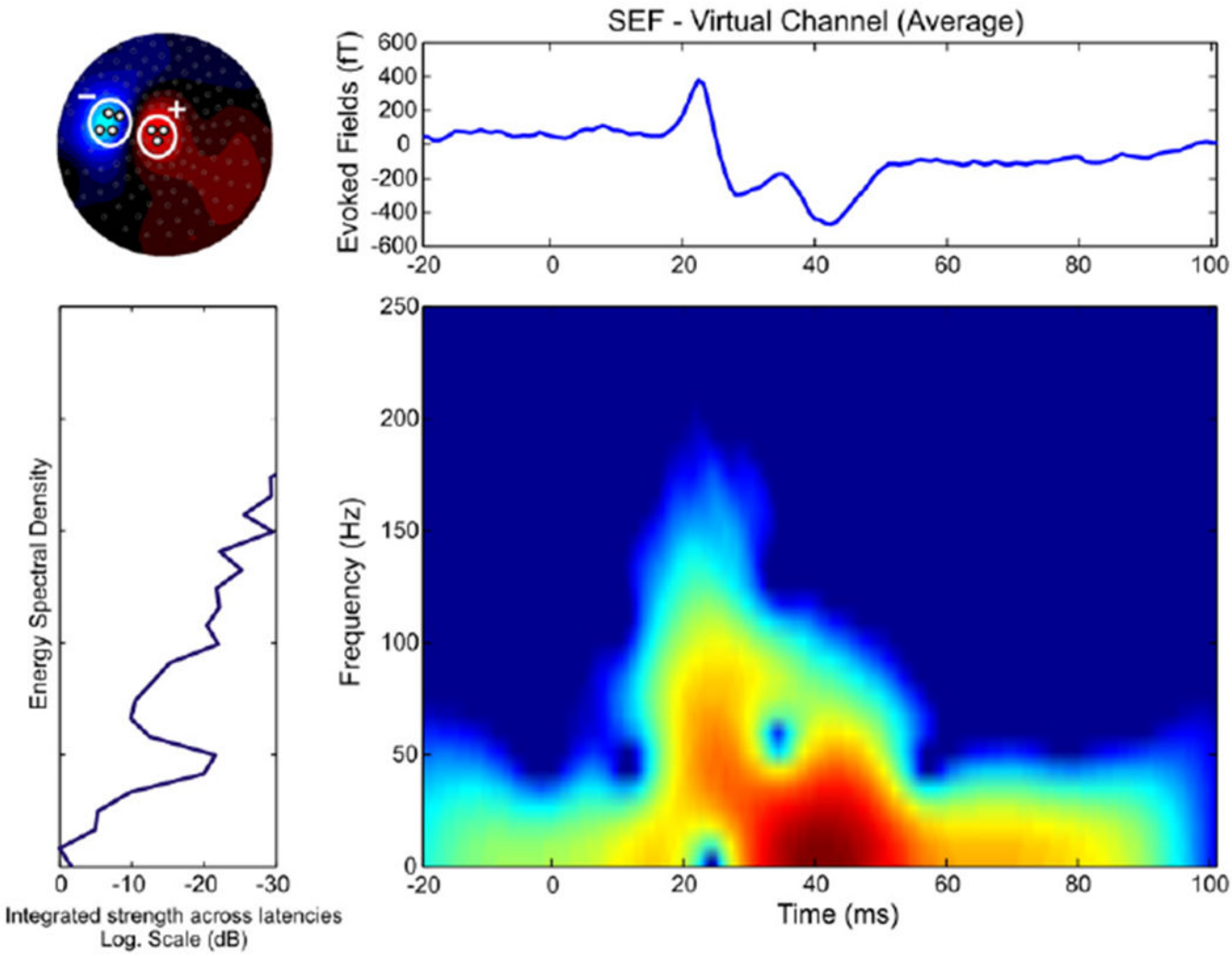

Fig. 1.

Time-frequency representation map for virtual channel estimated by SEFs (right wrist stimulation, one subject, averaged data among the two runs) for the whole frequency band (0–250 Hz). Left upper panel — the virtual channel was estimated at the peak of N20 by the difference between the MEG signals from sensors covering the peak magnetic flux entering the head (three sensors here) and exiting the head (four sensors here). Right upper panel — the virtual channel (in fT). Left lower panel — the energy spectral density of the virtual channel signal (in dB). Right lower panel — the time-frequency map (frequency range from 0 to 250 Hz).

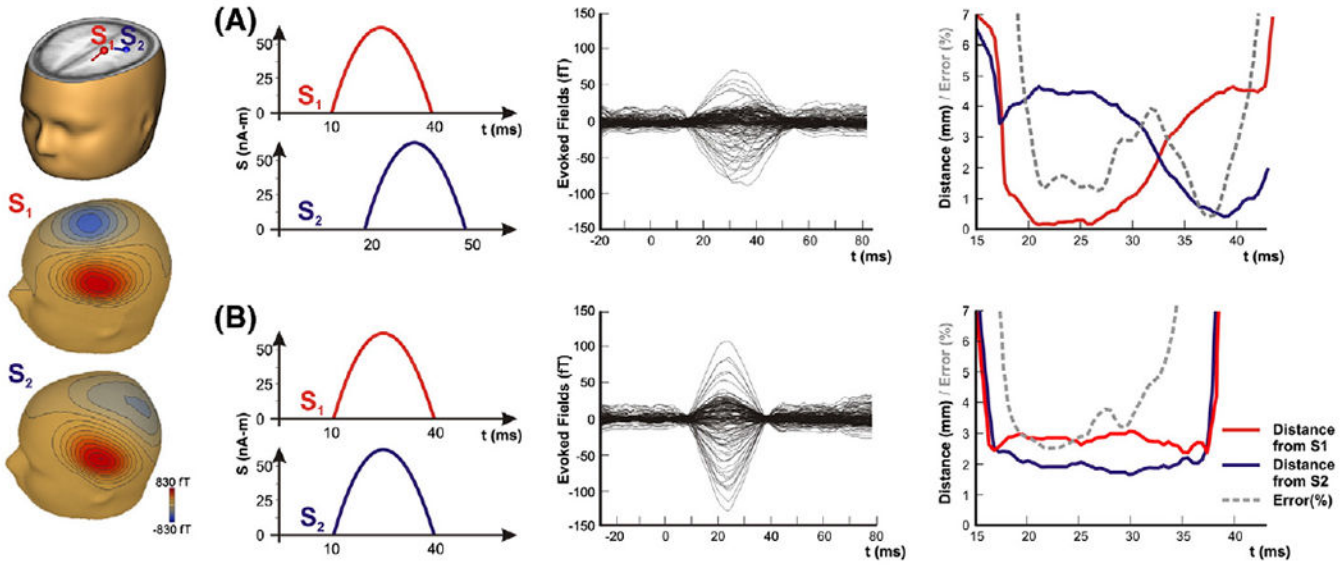

Fig. 2.

Simulation data using two dipolar sources S_1 and S_2. On the left column, the location of the two sources in a human brain model, and the magnetic flux generated on the sensor level by each source separately. Two cases were examined: (A) when the S_1 and S_2 were active serially with only partial temporal overlap, and (B) when they were perfectly synchronized in time. Third column — averaged magnetic fields (in fT) filtered in the 0–250 Hz. Fourth column — distance (in mm) between the estimated ECD and the dipolar sources S_1 (red line) and S_2 (blue line). Error (%) of fit with dashed grey line.

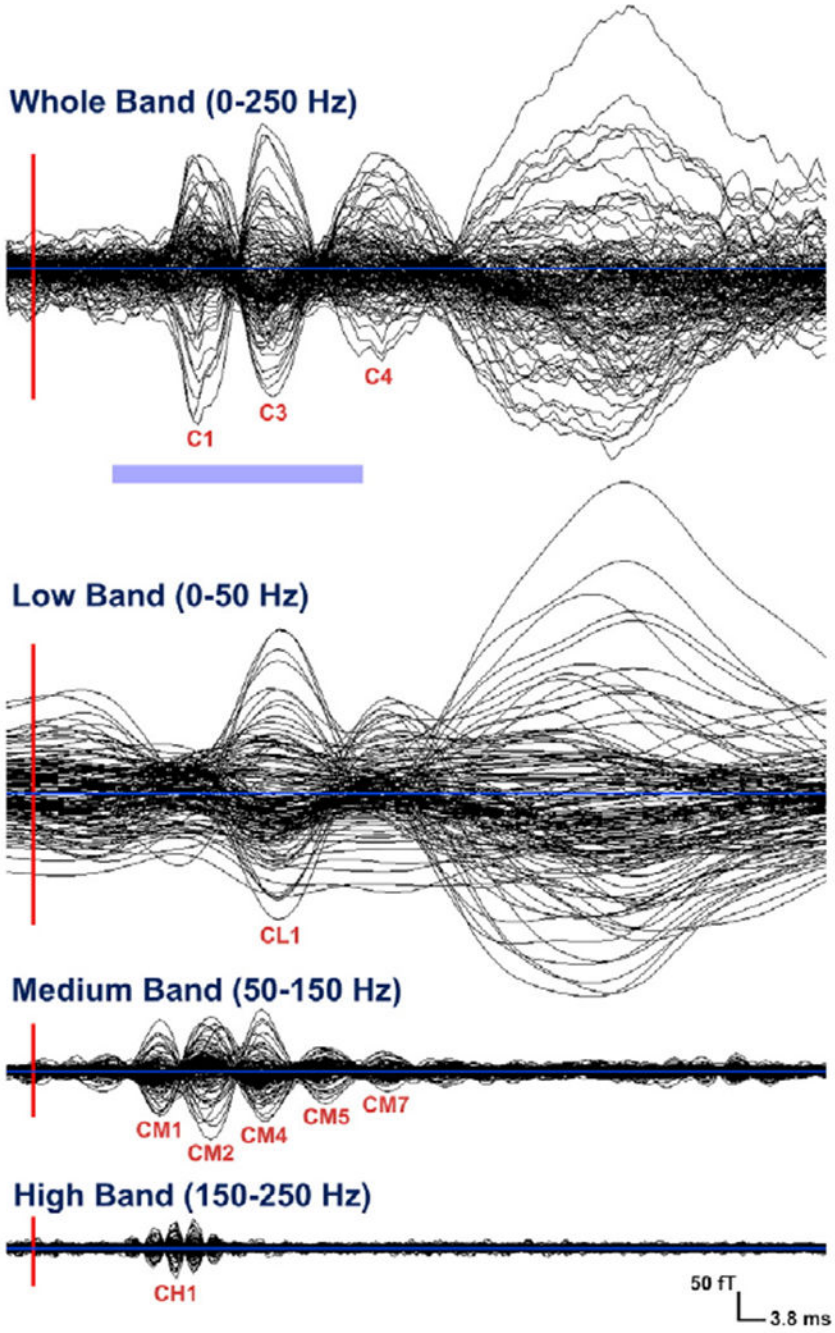

Fig. 3.

Averaged SEFs from left median nerve stimulation (one subject — one run) filtered in four different frequency bands: whole-band, low-band, medium-band, and high-band. Display from −3.8 up to 114 ms. The red lines mark the onset of the stimulus (vertical line) and the light blue line the zero level of the signal (horizontal line). The light blue bar below the whole-band averaged SEFs indicates the short-latencies in which the analysis was performed (from 10 to 40 ms).

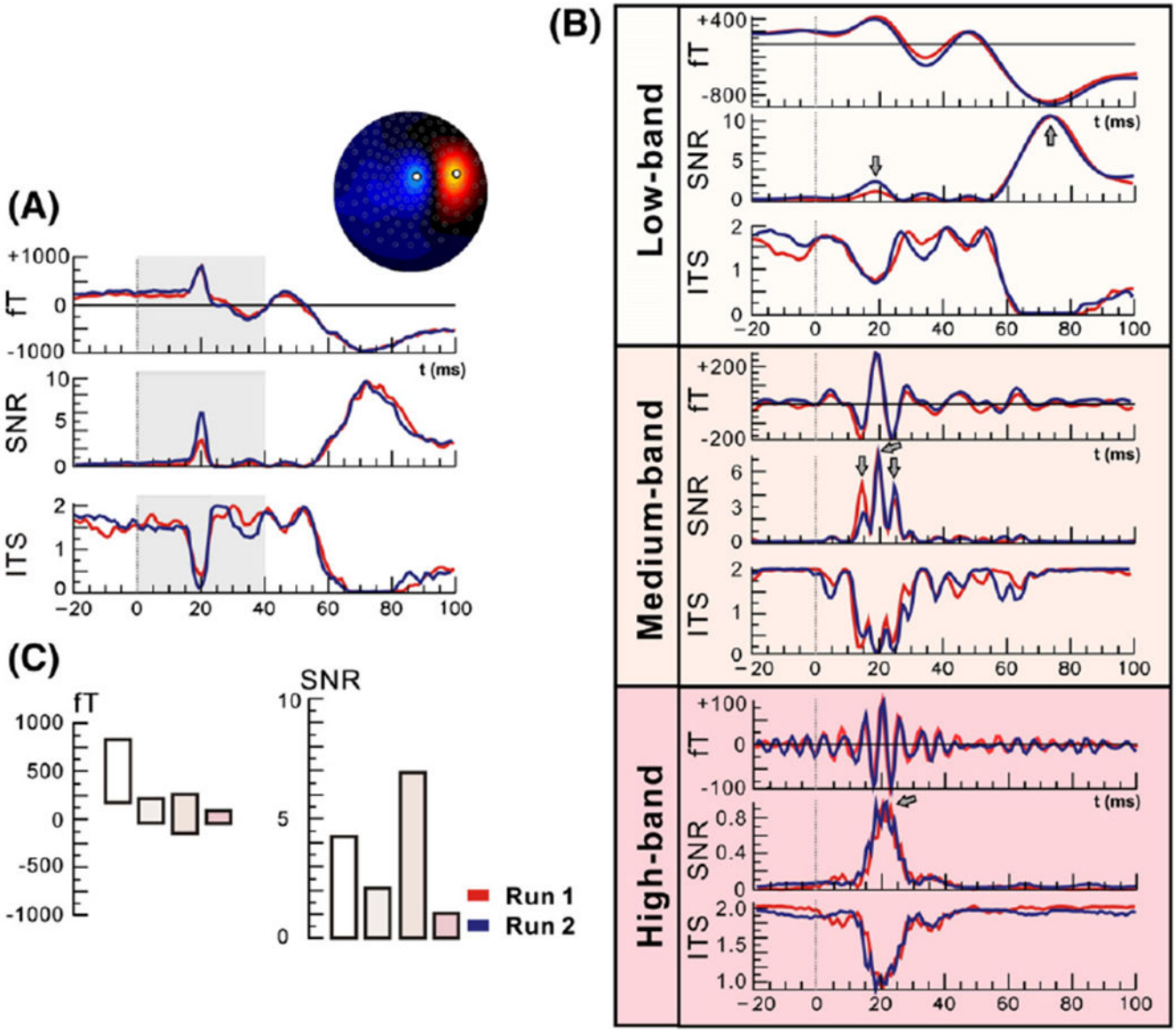

Fig. 4.

SEFs (in fT), SNR, and ITS of virtual channel (right wrist stimulation, one subject) for the whole frequency band (0–250 Hz) (A), and the low-band (0–50 Hz), medium-band (50–150 Hz), and high-band (150–250 Hz) (B) for two runs. The virtual channel was defined from the field map during the peak ofN20. (C) Displays derived from the same virtual channel at the peak ofM20 of peak-to-peak SEFs values (in fT) on the left and SNR on the right (averages between two runs). In each case the values displayed are in turn for the whole-band, the low-band, the medium-band and the high-band following the colors for each band as appear in (B). Note that the medium-band produces the highest SNR for the M20.

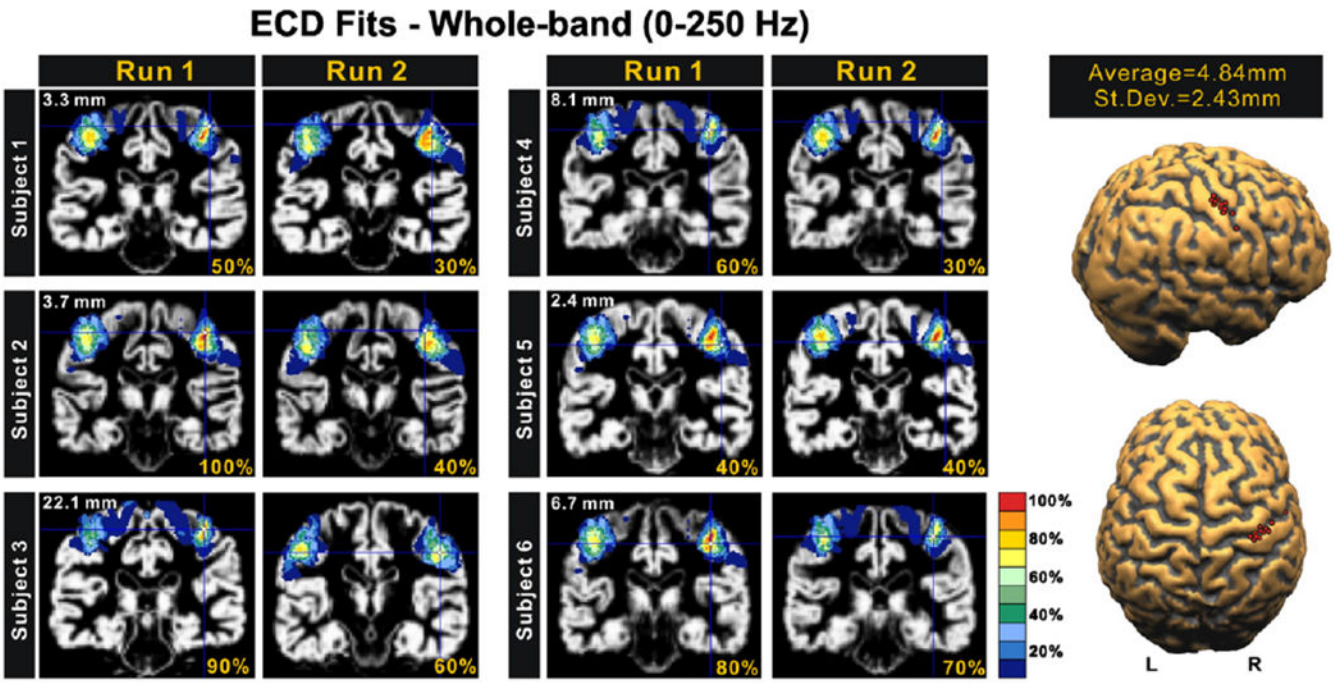

Fig. 5.

Correspondence of estimated generators at the peak of N20 to cytoarchitectonic areas for all subjects. For each subject the results for the two runs with left wrist stimulation are displayed. The ECD source estimates are shown by the cross-hair on each subject's MRI and over-plotted with the color-coded PCM for BA3b. The percentage value at the bottom of each subfigure is the probability for BA3b allocation at the MNI coordinate corresponding to the ECD (cross-hair) location. The number on the left upper corner of each pair of subfigure is the difference in source localisation between the two runs. The far right figures show the ECD estimates for the source in each hemisphere for all 12 runs (two for each subject) with the mean and S.D. of the separation of the ECD estimates in the two runs.

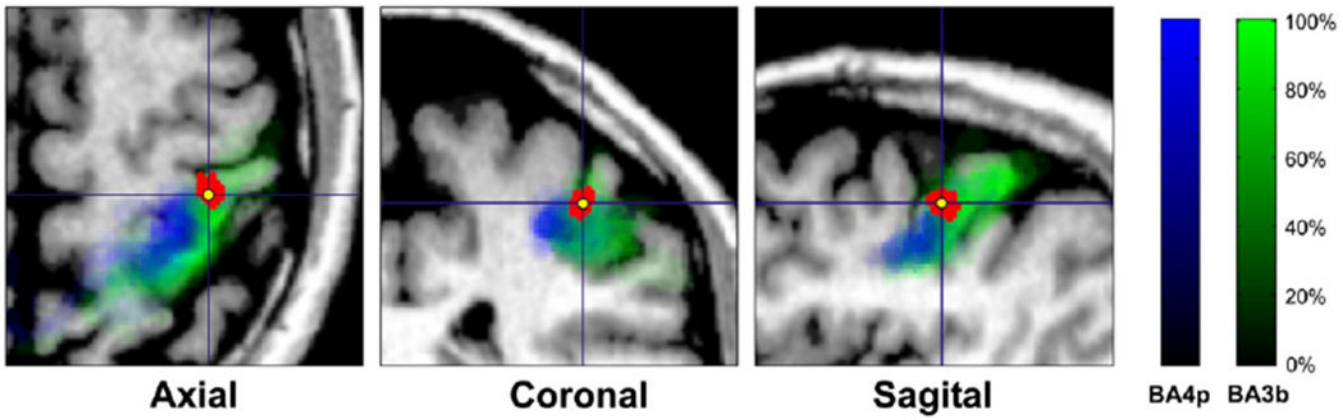

Fig. 6.

Correspondence of Monte-Carlo simulation generators at the peak of N20 to the cytoarchitectonic areas BA4p (blue color map) and BA3b (green color map) for a single subject (one run). The 500 dipole fit iterations form a dipole cloud displayed with red on the three anatomical views (axial, coronal, and sagittal); its center of gravity is displayed as the yellow point.

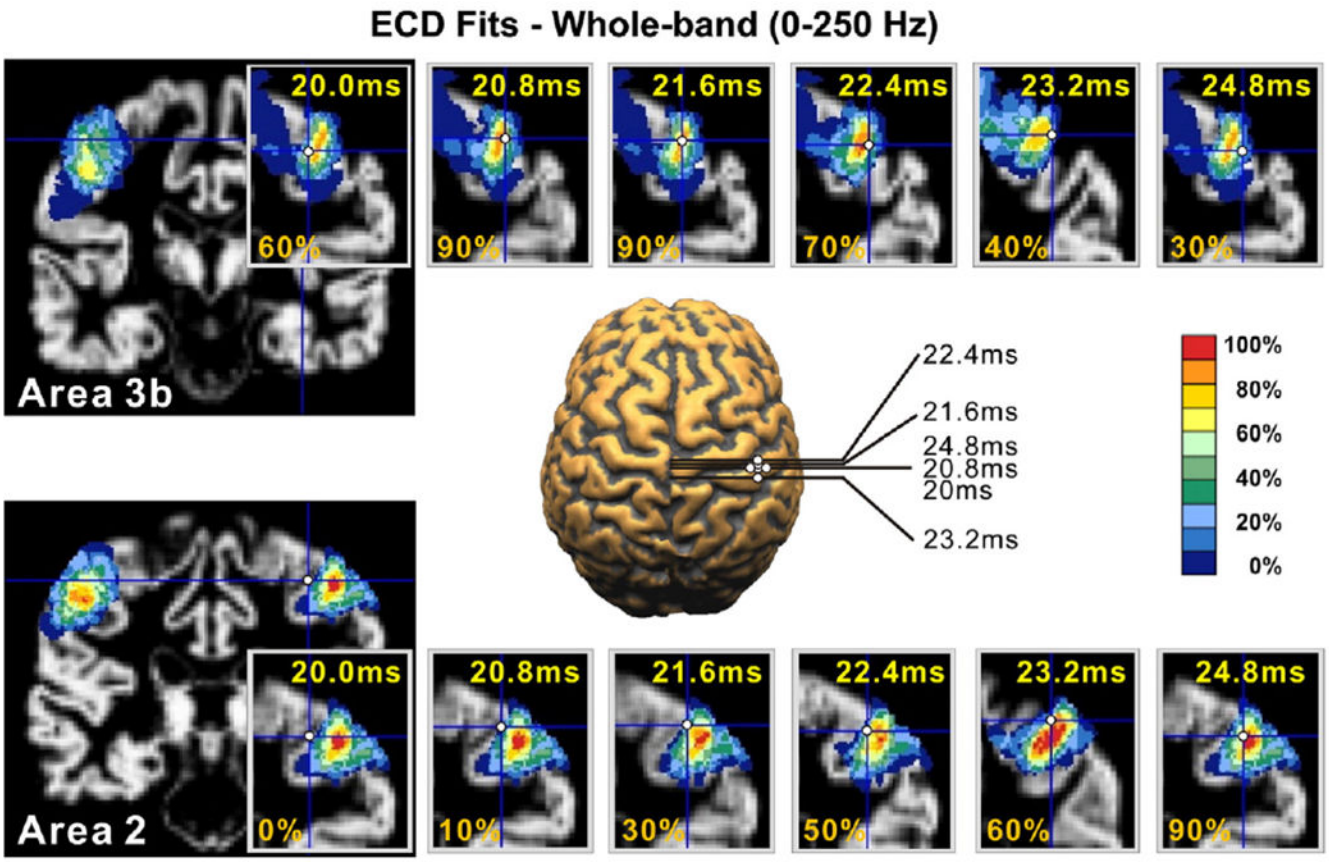

Fig. 7.

The time dependence of the ECD source estimate over-plotted on the subject's MRI and the PCMs for all time-points from 20 to 24.8 ms (subject 3, run 1, left wrist stimulation) for the whole-band (0–250 Hz). The top row shows the ECD estimates with the PCM map for area BA3b in a coronal slice that captures best the variation of the PCM for area BA3b. The bottom row shows the same information but for the area BA2. The larger plot in the middle shows the ECD estimate for some latencies on a segmented brain.

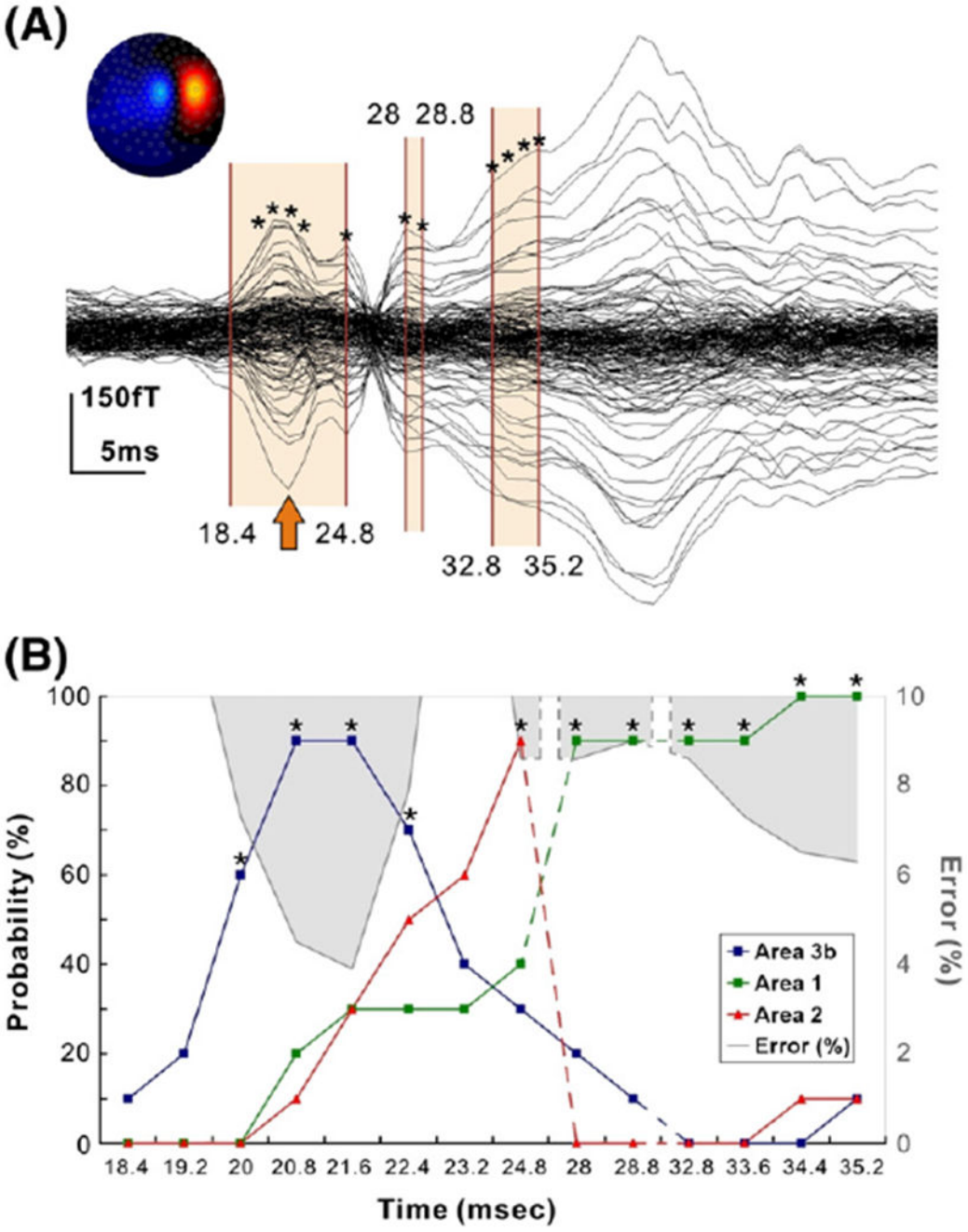

Fig. 8.

(A) Averaged SEFs (in fT) from left median nerve stimulation (subject 3, run 1, left wrist stimulation) filtered in the whole frequency band of 0–250 Hz. Contour map shows iso-magnetic fields during the N20 peak (indicated with an arrow), a single dipolar pattern over the right somatosensory area. Shaded areas indicate the time-ranges at which the ECD results are displayed on the lower panel. Asterisks indicate the time-points at which the ECD was fitted with GOF <90%. (B) For each ECD solution the estimated location is represented in MNI coordinates and the probability (%) of the PCM maps for that location to belong to

specific cytoarchitectonic areas is computed and displayed in the diagram for BA3b (blue), BA1 (green) and BA2 (red). The grey shaded areas show the values of localisation error (%) = 100 — GOF for the ECD at each time-point. It is evident that high GOF (low error) is correlated with activity in one cytoarchitectonic area.

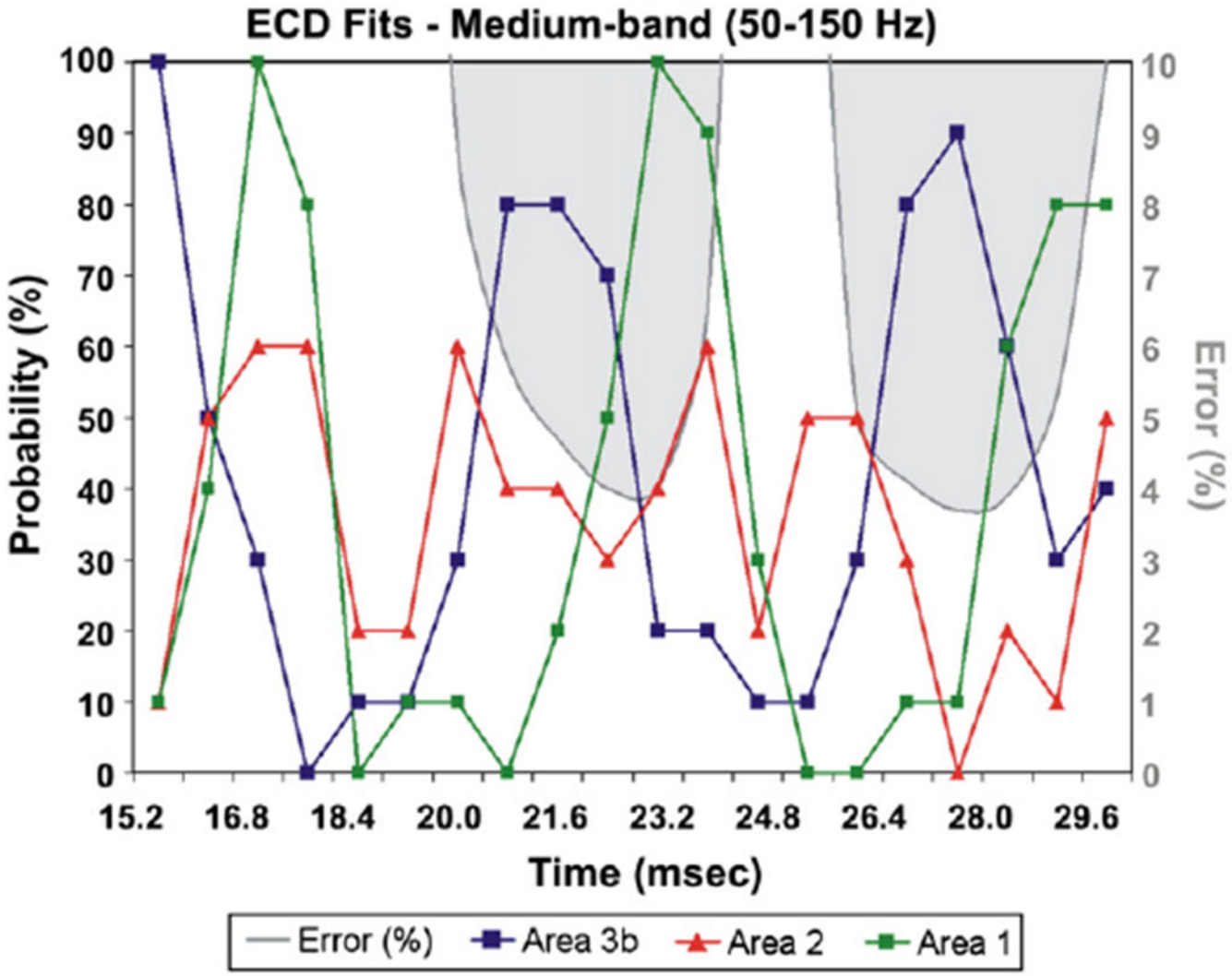

Fig. 9.

The PCM and GOF variation of the ECD solutions, fitted to the data filtered in the medium-band, for each time-point from 15.2 to 31.2 ms (subject 3, run 1, right wrist stimulation). For each latency, the ECD location is transferred to the MNI coordinate system and the probability (%) of the PCM is computed and displayed for areas BA3b, BA1 and BA2. The same conventions as for the lower part of Fig. 5. Note again that high goodness of fit corresponds either to cases where one area dominates (e.g. BA3b around 21 ms) or two nearby areas (transitions between 21 and 24 ms and 27 and 29 ms).

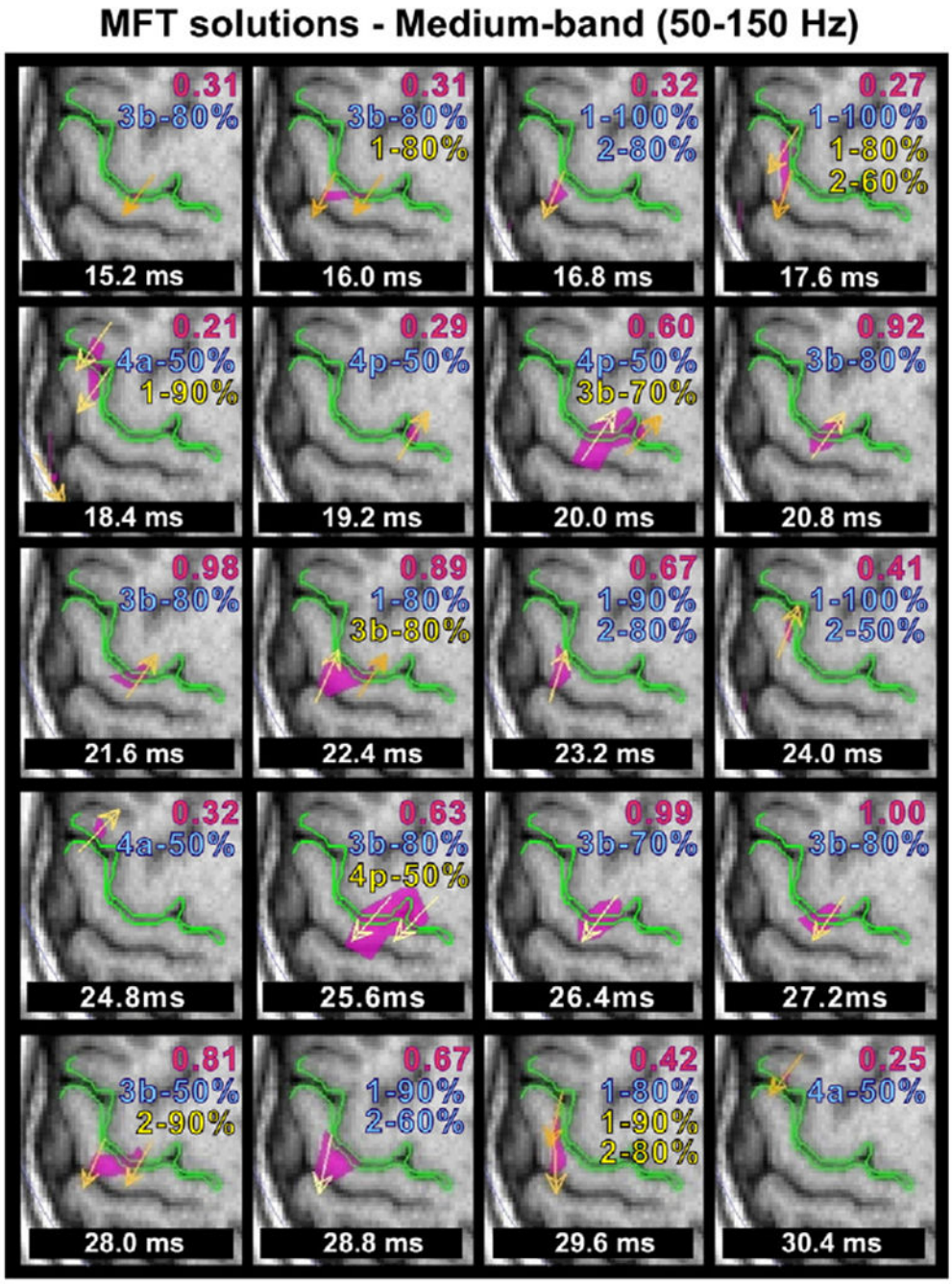

Fig. 10.

MFT localisation results for the medium-band (same dataset as in Fig. 6) from 15.2 to 30.4 ms. The overall maximum activity (modulus of the current density vector) in this range is at 27.2 ms, and for comparison the ratio of the maximum at each latency relative to the overall maximum is displayed at the right top corner of each subfigure with red font. Below this value the PCM values of the location(s) of the peak modulus are printed for the cytoarchitectonic areas BA3b, BA4a, BA4p, BA1, and BA2. Blue fonts are used for the % probability corresponding to the strongest source. For timeslices with more than one strong

peaks, yellow font is used for the corresponding PCM values at the location of the second source.

Table 1

Mean±S.D. latency (in ms) of each cortical activity observed at the four different frequency bands. Cmp: component. Runs: number of runs in which the component was present (all: 12 runs).

Left wrist			Right wrist	
Cmp	**Latency (ms)**	**Runs**	**Latency (ms)**	**Runs**
Whole-band (0–250 Hz)				
C1	21.32±0.85	All	21.83±0.69	All
C2	24.98±0.53	7/12	25.6±0.0	7/12
C3	31.85±2.68	All	31.53±2.16	All
C4	44.4±3.54	All	46.95±3.73	11/12
Low-band (0–50 Hz)				
CL1	34.4±1.13	8/12	34.24±2.09	9/12
Medium-band (50–150Hz)				
CM1	16.47±0.93	8/12	16.9±0.57	9/12
CM2	21.7±1.31	All	22.77±0.74	All
CM3	25.2±1.42	10/12	26.4±0.0	10/12
CM4	30.3±1.59	All	30.25±1.35	All
CM5	36.1±0.94	9/12	37.0±0.9	8/12
CM6	40.8±1.75	8/12	41.8±1.82	8/12
CM7	44.93±1.98	8/12	46.7±0.39	8/12
High-band (150–250 Hz)				
CH1	20.4±1.82	All	21.82±0.55	All

Table 2

MNI coordinates of ECD fits at N20 peak for the whole-band and the medium-band (left wrist stimulation) for all subjects and all runs, the corresponding cytoarchitectonic probabilities (CP) for BA3b, and the GOF. Mean values in bold.

Area 3b (whole-band, 0–250 Hz)										
Run 1						**Run 2**				
	x	**y**	**z**	**CP**	**GOF**	**x**	**y**	**z**	**CP**	**GOF**
Left wrist stimulation										
Subj1	46	−27	59	50	98.2	45	−24	60	30	96
Subj2	43	−25	55	100	96.1	40	−23	56	40	90
Subj3	42	−30	58	90	95.3	51	−19	41	60	87.3
Subj4	40	−29	56	60	91.2	45	−27	62	30	93
Subj5	49	−25	46	40	94.2	48	−26	48	40	95.3
Subj6	42	−25	48	80	94.8	40	−29	53	70	94.2
	43.7	**−26.8**	**53.7**	**70.0**	**95.0**	**44.8**	**−24.7**	**53.3**	**45.0**	**92.6**
Area 3b (medium-band, 50–150 Hz)										
Subj1	44	−28	58	70	97.2	42	−29	61	70	97.5
Subj2	43	−29	64	60	96.74	44	−26	60	60	94.3
Subj3	50	−23	44	60	96.9	45	−25	52	70	96.1
Subj4	40	−28	51	90	96.19	41	−29	53	90	97
Subj5	37	−39	63	80	94.12	40	−36	60	80	95.3
Subj6	41	−29	53	90	97.14	40	−29	55	60	94.3
	42.5	**−29.3**	**55.4**	**75.0**	**96.4**	**42.0**	**−29.0**	**56.8**	**71.7**	**95.8**